

Metamaterials and their applications: An overview

Ali Valipour¹, Mohammad H Kargozarfard¹, Mina Rakhshi¹,
Amin Yaghoontian¹ and Hamid M Sedighi^{1,2} 

Proc IMechE Part L:
J Materials: Design and Applications
0(0) 1–40
© IMechE 2021
Article reuse guidelines:
sagepub.com/journals-permissions
DOI: [10.1177/1464420721995858](https://doi.org/10.1177/1464420721995858)
jmd.sagepub.com/home/pil



Abstract

Metamaterials are man-made substances with unique spatial alternations in their constituent components. They are widely used in modifying elastic, acoustic, or electromagnetic properties of materials. Metamaterials induce low/high-frequency band gaps to control wave propagations with different wavelengths and are also frequently applied in microwave engineering, waveguides, dispersion compensation, smart antennas, and lenses. For instance, permittivity and permeability of the metamaterials can take positive or negative values. Due to smaller single-cell dimensions than their wavelength, the selective frequency of surface-based metamaterials is used for waveguiding. The need for adjustable bandgaps can also lead to a plethora of research into metamaterials' tunability for structures that operate at different speeds. In this article, recent studies in the field of metamaterials and their applications are reviewed. The piezoelectric metamaterials and the electromagnetic metamaterials are introduced that is followed by a review of new types of chiral metamaterials. Additionally, absorber, nonlinear, terahertz, tunable, photonic, selective surface-based frequency in acoustic metamaterials are compared and some remarks on tuning bandgaps methods in locally resonant metamaterials are provided.

Keywords

Metamaterial, periodic composite, acoustic wave, chiral, local resonance, phononic

Date received: 29 October 2020; accepted: 29 January 2021

Introduction

Metamaterials are a new class of artificial compound materials, which exhibit exceptional properties not found in naturally occurring materials. The metamaterials have spatial alternation in boundary conditions or phases of the constituent components or geometry. The attempts by Newton to describe sound propagation in air and by Riley to study alternating structures are some of the earliest records of metamaterials in the fields of vibrations and acoustics. Acoustic metamaterials (AMs) have attracted growing interest over the past few decades because of the improvements in sound wave field measurement and feedback vibration, which could not be done with ordinary materials.¹

The usual arrangement of these materials is based on components that are periodically and regularly embedded in the base environment. AMs can have a negative modulus of elasticity, negative density, or anisotropic mass. These capabilities caused metamaterials to be in high demand and provided an unprecedented way to manipulate wave propagation and vibration. In AMs, the embedded components are

generally called resonators. Transitional and rotational resonators are two common types of resonators found in metamaterials, which can effectively change density and elasticity. Unlike conventional materials, the resultant properties are a function of frequency, mass, and elastic components, which leads to achieving negative properties at a specific frequency range. There are double-negative metamaterial systems, which exhibit negative refractive index and are created by combining two resonators. That essentially stems from having group and phase velocities with opposite signs. The double-negative metamaterial is usually referred to as the left-handed AMs or the negative indicator material. Here is an overview of the

¹Mechanical Engineering Department, Faculty of Engineering, Shahid Chamran University of Ahvaz, Ahvaz, Iran

²Drilling Center of Excellence and Research Center, Shahid Chamran University of Ahvaz, Ahvaz, Iran

Corresponding author:

Hamid M Sedighi, Shahid Chamran University of Ahvaz, Faculty of Engineering, Golestan, Ahwaz, Iran.

Email: h.msedighi@scu.ac.ir

materials with effective negative mass, negative elasticity, and double-negative material (Figure 1).²

The applications of metamaterials are found in different fields including public safety, sensor identification, high-frequency battlefield communications, improved ultrasonic sensors, solar energy management for high-gain antennas, and remote aerospace applications.^{3–5} The army and air force researchers use metamaterials to detect the presence of explosives, biological materials, and contamination.^{6–10} Metamaterials easily manipulate sound wavelengths that are much larger than light. Sound bends around it provided by Navy Researcher, which may be used to hide submarines in military applications. Civilian spin-offs also use metamaterials to produce sound chambers. Army engineers use metamaterials to make small and high-speed photonic equipment as light is replacing electricity in the future circuit boards.¹¹

Nano-scale metamaterials are used to control optical or acoustic signals that improve ultrasound resolution and discoloration of materials. These materials can be prepared by a multilayer deposition process with high precision. The thickness of each layer can be controlled by using a fraction of the wavelength. Biosensors are essential tools in many fields to study biological phenomena such as environmental monitoring, food safety, and disease detection. In the past, fluorescence-based methods have been used by researchers in bioassay technologies; however, recently, metamaterials have been used because of the discovery of cost-effective biomolecules. Absorbent metamaterials absorb electromagnetic radiation effectively. Metamaterials are also utilized in antennas to increase the efficiency of the shrinking antenna system. Metamaterial antennas are used to improve an antenna's utilization because of their exceptional bandwidth characteristics and alternating structure. Conventional small antennas reflect the highest signal wavelength to the source. However, the metamaterial antenna has a design that stores energy and re-radiates, causing a small-sized antenna to behave as a more extensive antenna.¹²

Another type of metamaterials is tunable metamaterials. These metamaterials have the ability to change the frequency of a refractive index randomly. An electromagnetic wave with these metamaterials gives a variable response. The structure of tunable metamaterials can be modified to allow the device to be reset during operation. The change near the infrared range is achieved by changing the permeability of the liquid crystal. Negative index values in metamaterials can be increased or decreased or set to positive or zero-index values. Metamaterials have many types and have many applications. Electromagnetic, chiral, terahertz, piezoelectric, photonic, tunable, acoustic, and nonlinear metamaterials are different types of metamaterials. The concept of metamaterial structure with damp vibrations is based on embedding the local resonance

systems in a single-cell structure. The resulting alternating structure can be treated as a material with dynamic properties to be exploited in the various engineering fields.

This article is aimed at providing an overview of recent developments on metamaterials and their applications. To this end, after introducing the piezoelectric metamaterials and electromagnetic metamaterials, the new types of chiral metamaterials are investigated. Because of the importance of chiral metamaterials, they are described separately. Then, an attempt has been made to review the studies on the absorber, nonlinear, terahertz, tunable, photonic, frequency-selective surface-based metamaterial, and AMs. In the end, the methods of bandgap tuning in the local resonance metamaterials are discussed in detail.

Metamaterial definition

The metamaterials concept emerged within the late 1990s and was first used officially by the Defense Advanced Research Projects Agency Symposium on Meta-Materials in 1999. The pioneers originated it within the field by using the prefix meta, which is loanwords from the Greek language with the meanings of "after" or "beyond," signifying that metamaterials are more comprehensive or transcending than the ordinary material with exotic properties not observable in nature. Metamaterials are a novel class of complex composite materials that have produced tremendous interest due to their ability to exhibit any desirable electromagnetic, acoustic, or mechanical property such as negative mass, stiffness, or Poisson's ratio under specific circumstances. The physics of these advanced materials and associated concepts have triggered intense discussions and produced a scientific eruption.¹³

Metamaterials are artificially engineered materials to supply properties that "may not be readily available in nature." Instead of composition, these remarkable properties are obtained from the structure using small inhomogeneities to implement efficient macroscopic behavior. Metamaterials can exhibit strange electronic, thermal, magnetic, acoustic, or elastic properties; however, in this effort, we focus our attention on acoustic and elastic properties. Metamaterials are also referred to as "artificial composite structures," and composites are usually composed of two or more chemically/physically different phases, separated by a definite interface. On the opposite hand, metamaterial consists of periodic cells with two or more physically different mechanisms that provide properties that are not found in naturally formed substances. Also, architectural structures significantly truncate the border of metamaterial definition.

Metamaterials form a broad class of composite structures with constituting artificial inclusions

named unit cells. There is no globally accepted definition of AMs, however. The word “acoustic metamaterial” sometimes solely refers to a “locally resonant periodic material,” while other times include PCs with Bragg-scattering. A unanimously defined metamaterial is that they are rationally designed artificial structures periodically arranged, exhibiting unusual intrinsic properties.¹⁴ This human-made composite manages structural behavior and dynamic properties and has found its applications within the areas of cloaking, imaging, energy harvesting, and noise and vibration control, among others.

The phononic crystal (PC) is an influential and elder group entitled in analogy to their counterpart, photonic crystal, and forms a major group of metamaterials. The PC term is used to explain materials with elastic inclusions inside a particular matrix. The anomalous behavior in PCs arises from interference of waves strongly scattered off the inclusions and transmitted through the inclusions and matrix. This group length should be a minimum of one half a wavelength and described by Bragg scattering concepts. The critical dimensions of a bandgap material are directly linked to the wavelengths to interact with it strongly.

The distinctive characteristics of AMs originate from a resonator component that is located within each unit cell. Their abnormal material properties are owned by mechanical oscillators driven through resonance, which abruptly change or transform a share of input energy. Therefore, the displacement amplitude becomes large in low-loss materials. The reliance on the resonance frequency of the geometry, including lattice parameters and incidence orientation, is an essential distinction between locally resonant sonic materials and PCs. PCs require the wavelength at the bandgap center frequency to get to the lattice constants’ order within the propagation direction. However, each device includes its mechanical oscillator in the AM. This function makes the size of unit cells tiny and has limited crosstalk, making private frequencies of each individual resonator insensitive to lattice parameters and direction.¹⁵ The wavenumber change curve in terms of frequency is called the dispersion curve, and the spatial frequency in the vibrational response of a system is called the wavenumber. The frequency range in the system where no vibration is transmitted is called the stopband, and the frequency corresponding to the lower limit of the stopband is also called the target frequency.

Piezoelectric metamaterials

The exotically engineered piezoelectric structures are a crucial target for the development of desired properties in metamaterials. Piezoelectric materials are most widely used in micro-electromechanical systems (MEMS) and intelligent sensors because of their

excellent flexibility and tunable mechanical properties. Due to the piezoelectric property, energy can be converted between electrical and mechanical domains. It allows the apparatus to optimize the bandgap (size and location) and harness the input energy flow. Therefore, due to their unique electro-mechanical coupling characteristics, piezoelectric materials play a vital role in the industry of advanced multipurpose composites. Piezoelectric materials have applications in actuators, sensors, ultrasound imaging, hydrophones, and echocardiograms. In these devices, piezoelectricity converts mechanical energy into electrical energy.

In 2019, Khan et al.¹⁶ analyzed the piezoelectric metamaterials with negative and zero Poisson ratios. They proposed a finite element-based micromechanical modeling method to determine the electromechanical properties of piezoelectric metamaterials with a honeycomb network. Structure symmetry was used to obtain the hybrid boundary conditions similar to the alternating boundary conditions. Three categories of honeycomb networks, namely regular honeycomb, inner honeycomb, and semi-inward honeycomb, were considered. The volumetric elements of these three types of cellular materials were created, and finite element simulations were performed to analyze the effects of orientation of the joints on the useful electromechanical properties. Piezoelectric longitudinally implanted cell networks were shown to behave more advanced than monolithic piezoelectric materials. The results reveal that cellular metamaterials could be developed with tunable electromechanical parameters and different mechanical behavior such as positive, negative, or zero Poisson ratio. Such cellular materials with honeycomb networks are likely to facilitate lightweight devices for various next-generation sensors and actuators. In their paper, three types of piezoelectric metamaterials were considered (Figure 2). These cell networks could exhibit different acoustic behavior, including positive, negative, and zero Poisson ratios.

First, the linearized equations governing the piezoelectric cellular material constitutive model were extracted. Next, the finite element model of honeycomb cellular material was formed by varying the ligament orientation between 30 and 60%, which corresponds to the porosity values of 50–85%. Finite element analysis was performed using ABAQUS software. Soft piezoelectric material with specific electromechanical properties was considered as the basic structure for the cellular material. The finite element model with specified boundary conditions is illustrated in Figure 3. In this model, each node has four degrees of freedom. To prevent rigid body movement under electrical loading, points A, B, and C were explicitly restricted. The location of these points has been shown in the figure. The cellular materials were assumed to be polarized longitudinally

and transversely, and each region was polarized uniformly.

In general, a finite element-based micromechanical model was presented for estimating the piezoelectric, dielectric, and elastic properties of honeycomb cells.

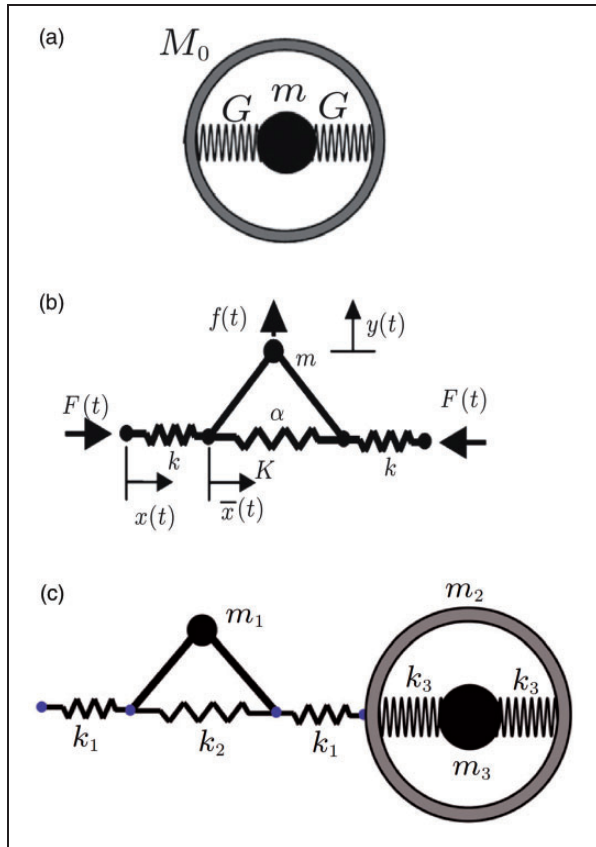


Figure 1. Effective negative mass, negative modulus, and doubly negative material.²

By using the alternating nature of structure and internal symmetries, a hybrid boundary condition similar to the alternating boundary condition was applied. The results showed that, for polarized grids in the longitudinal direction, the honeycomb grids could exhibit an exceptional combination of piezoelectric properties, low impedance, and higher sensitivity, which could not be achieved by integrated piezoelectric. However, for polarized grids in the transverse direction, the electromechanical properties showed a slight dependence on the porosity and ligament angle. The finite element results were shown that the honeycomb grids could be produced with tunable electro-mechanical properties coupled with the auxetic behavior, including negative or zero Poisson's ratio.

Zhu et al.¹⁷ proposed a metamaterial that controls bandgap position by using shoulder piezoelectric property. The shoulder piezoelectric converted some of the mechanical energy generated by vibration into electrical power. Piezoelectric led to the additional degree of freedom, transfer of structural working frequency, and the proposed tunability. The experimental results were tested over a wide range of transitional waves, and the performance of the proposed metamaterial in bandgap tuning was demonstrated. The proposed structure was considered an acrylic tube with I-shaped beams in the middle and a concentrated lead mass in the middle of the beam. One of the two ends of the beam was connected to the pipe by a shoulder piezoelectric. Figure 4 shows a schematic of the metamaterial. The elastic piezoelectric modulus and hardness of the beam could be controlled by inducing current to the established circuit. By increasing the current, the significant negative mass was shifted to the lower frequencies, and by decreasing the current, the significant negative mass

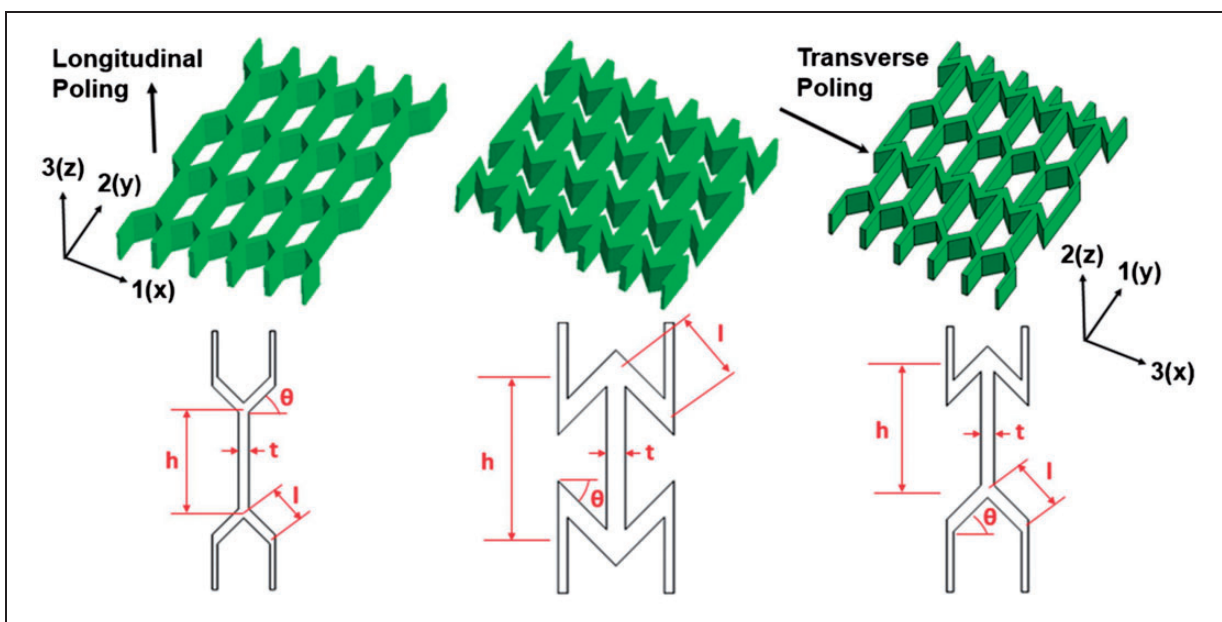


Figure 2. Piezoelectric cell grid with left-to-right honeycomb, intrinsic honeycomb, and semi-intrinsic honeycomb structures.¹⁶

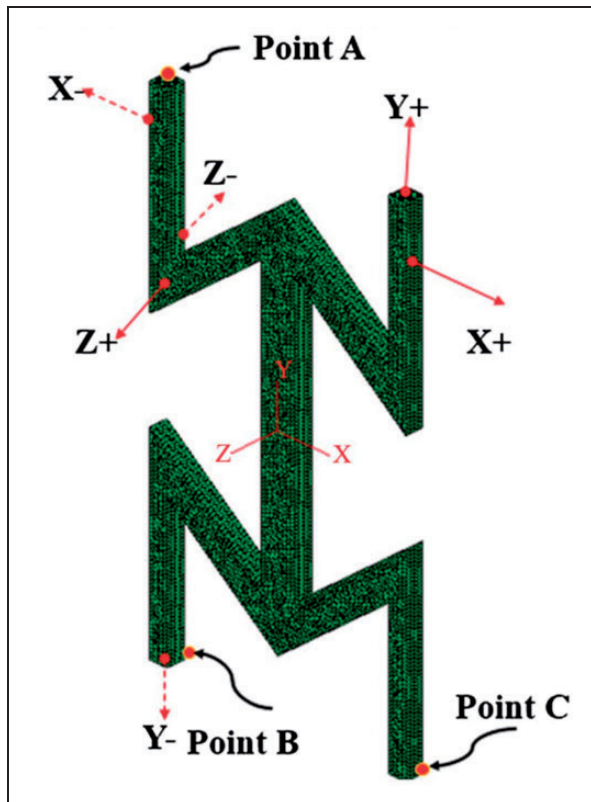


Figure 3. The single-cell meshed with ten node elements.¹⁶

was shifted to the higher frequencies. To confirm the proposed structure's properties, the structure was first tested by a mechanical shaker with harmonic vibrations. The designed circuit (current reducer or amplifier) was connected to the piezoelectric and the DC source. The test structure consisted of nine cells as described below, and the tenth cell consisted of an empty acrylic tube at the end of it for accelerometer placement.

Dimensionless bandwidth was defined as $(\omega_{\max}^* - \omega_{\min}^*)$ and was increased up to 45% in this experiment. The impact test was then used to simulate the explosion wave. Thus, a pendulum with a 15° swing angle and aluminum mass impacted the metamaterial in three different directions. The results were used to measure the impact wave before and after the impact of two miniature piezoelectric sensors (WFB, APC International, Ltd., P-6.36 mm-0.33 mm-850). Despite the complexity of the results, the impact intensity in all three cases decreased significantly, indicating that the explosion-proof vest design was acceptable.

Several metamaterial beam elements, coupled with piezoelectric elements embedded in each, were presented by Hu et al.¹⁸ Recent research showed that there was an additional gap in the model. Since the bandgap determined the vibration reduction performance, increasing the bandgap would cause the vibration reduction behavior of the structure to be improved. The idea of the metamaterial piezoelectric

beam was also presented in this article. They introduced the Euler–Bernoulli beam theory and transfer matrix method to determine the complete bandgap. In the following, two finite element models were presented for realizing the beam. In the first model, each exciter was modeled as a spring and damper system. In the second model, each exciter was modeled with a beam. The results of both analytical models were compared with the Bernoulli beam results involving actuator piezoelectric, which showed that the second model was close to the actual beam conditions. The results of vibration reduction and energy harvesting in the beam were compared.

Chen et al.¹⁹ proposed a metamaterial-based sensing system with an array of piezoelectric patches and examined that using both numerical and experimental methods. The introduced system could overcome the detection limit by absorbing two orders of magnitude amplification of the flexural wave signals. This article combined the concepts of the acoustic rainbow-trapping metamaterial and adaptive systems with piezoelectric circuitry to enhance the quality and quantity of elastic waves for monitoring purposes. Shunted piezoelectric elements were used to control the metamaterial properties. Shunted circuits could continuously modify the resonant properties of the metamaterial over a wide frequency range. The schematic of the design metamaterial beam is shown below. According to the figure, this adaptive metamaterial was constructed by bonding a periodic array of piezoelectric patches on an aluminum beam. The patches were individually shunted with an array of gradient NC circuits to ensure a linear variation in the refractive index. PZTs could be easily tuned by adjusting a potentiometer. As seen in Figure 5(b), it is shown both theoretically and experimentally that by decreasing the frequency, waves traveled a long distance through the waveguide and then reflected out. The wave amplitude was dramatically diminished by increasing frequency, and low-velocity amplitudes were measured downstream of the metamaterial.

Matlack et al.²⁰ introduced a metastructure that used structural geometry to modify different local resonance modes instead of material properties selectively. Additionally, it could tune the stopband by local resonance. The structure consisted of a polycarbonate network with steel cubes embedded in it. These cubes acted as the local resonators. In their study, the bandwidth between the steel networks was determined, and the results were investigated in a practical and simulated manner. The facade introduced in this experiment is a beam (containing 12 beams with length L) made of polycarbonate. A solid steel cube set was embedded into the hollow space to reinforce this structure (Figure 6). By changing the density of the steels, the structural strength could be changed.

To measure the transmitted elastic waves, a three-dimensional print sample was made. The sample was fixed between a piezoelectric that excited the structure

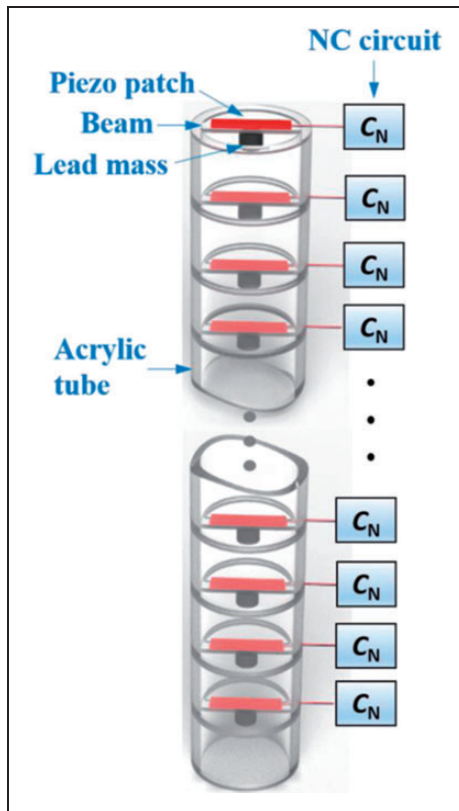


Figure 4. Proposed metamaterial with bandgap setting and piezoelectric properties.¹⁷

and a force sensor that calculated the motion in the x -direction. The lockable amplifier excited the piezactuator and measured the structural response. In order to keep the support conditions stable, it sometimes monitored the static force of a cell continuously pre-compressing the structure. The test conditions consisted of a fixed static force cell that was frictionless in the opposite direction of the dynamic force sensor, while the piezoelectric mounted on the propeller to control the pre-pressure force. To confirm the smooth response of structure within the frequency range of 1–10 kHz, the sample response was recorded by directly pressing the pressure sensor on the piezactuator with the same pre-pressure test force, which could be used to determine the system noise.

Nouh et al.²¹ introduced a tunable bandgap mechanism for a metamaterial structure. The internal resonator had an active piezoelectric composition. Additionally, the metamaterial unit cell consisted of a passive substrate filled with piezoelectric polyvinylidene fluoride membranes. The local resonance sources were small masses within the membranes. Changing the resonance properties of infrastructures could extend the bandwidth and move it to lower frequencies. In general, external electrical excitation tuned the structure's local resonance frequency by controlling the stiffness of the polyvinylidene fluoride membranes. The finite element method was used to understand the metastructure's behavior. Excitation

of polyvinylidene fluoride membrane caused in-plane forces. In this paper, these forces were formulated mathematically, and the concept of geometrical stiffness was used to investigate their influence on the flexural stiffness of the structure. The compounds that are presented in the metamaterial plane and the corresponding resonator in each unit cell are shown in Figure 7.

Popa et al.²² have suggested an active, physically fixed structure metamaterial to control the acoustic wave propagation. The metamaterial unit cell consisted of a three-terminal piezoelectric membrane, which generated an electric signal proportional to the received incident sound. The piezoelectrics manipulated the local sound field at the cell location and produced a form of delay via two reconfigurable electronic blocks, as seen in Figure 8.

By activating all delay lines, the linear superposition of the two operations was attained. More importantly, the plane wave and oriented beams leaving the metamaterial slab were almost identical to the beams of the primary devices. Such an integral functionality confirmed the excellent potential of the metamaterial slab to work simultaneously as two separate devices. The plane wave and centered beams leaving the metamaterial slab were almost identical to the beams of simple devices whose functionality was combined, confirming the slab's excellent ability to act simultaneously as two independent devices, as shown in Figure 9.

Sugino et al.²³ introduced a mechanical locally resonant metastructure by combining a piezoelectric bimorph beam with piezoelectric layers poled in an opposite transverse direction and a mass-spring resonator attached to each unit cell. While the mechanisms accounting for mechanical and electromechanical locally resonant bandgaps were radically different, hybrid bandgaps were generated by these two forms. These two distinct electrical and mechanical bandgaps were constructing three possible scenarios. First, each corresponding bandgap was a separate, locally resonant bandgap that leads to individual bandgaps. Second, if the two bandgap frequency ranges had an overlap, in the overlapping frequency range, a wave could propagate such that no bandgap could be detected in the overlapping frequencies other than the two non-overlapping regions. Third, if the two frequency ranges were tuned to be almost adjacent, a single wide bandgap emerged, as can be seen in Figure 10.

Electromagnetic metamaterials

Over the past few years, the field of electricity and magnets has gained considerable attention as the ways to modify material properties have improved. This concept embarks on the development of electromagnetic metamaterials as a new class of materials encouraging a greater variety of component

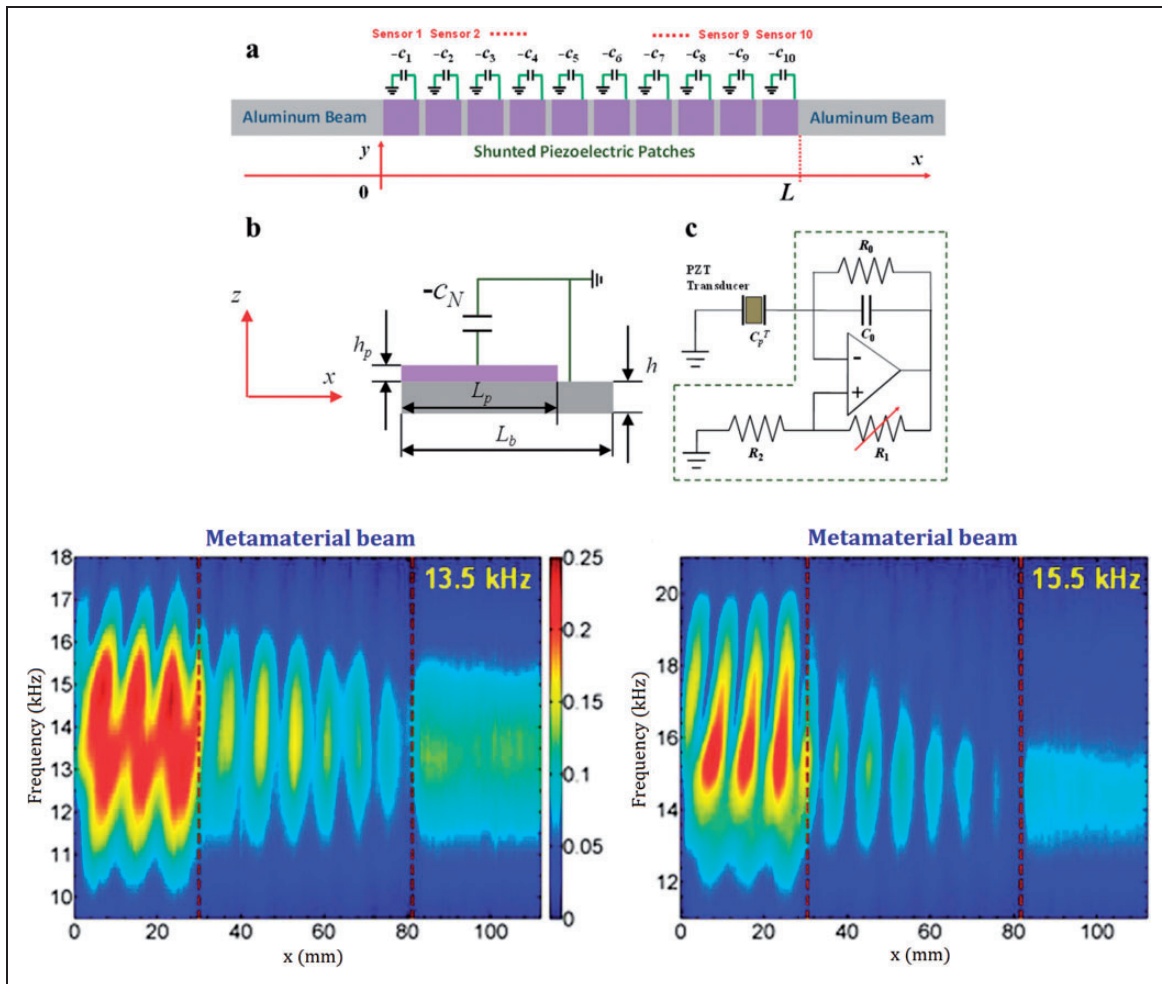


Figure 5. (a) Schematic of the adaptive GRIN metamaterial beam design¹⁹ and (b) reflected waves through waveguide.¹⁹

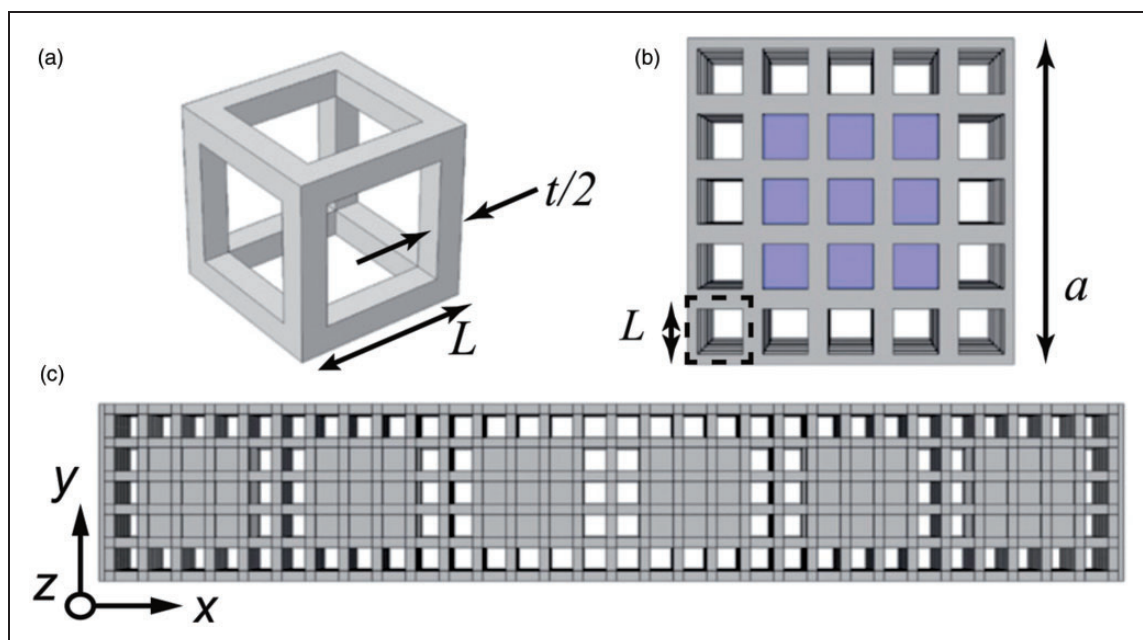


Figure 6. Single-cell counter made by a 3D printing method.²⁰

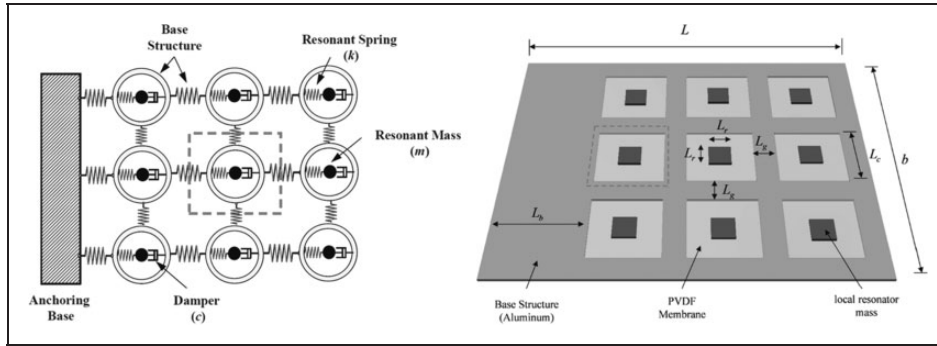


Figure 7. Metamaterial plate and corresponding resonator.²¹

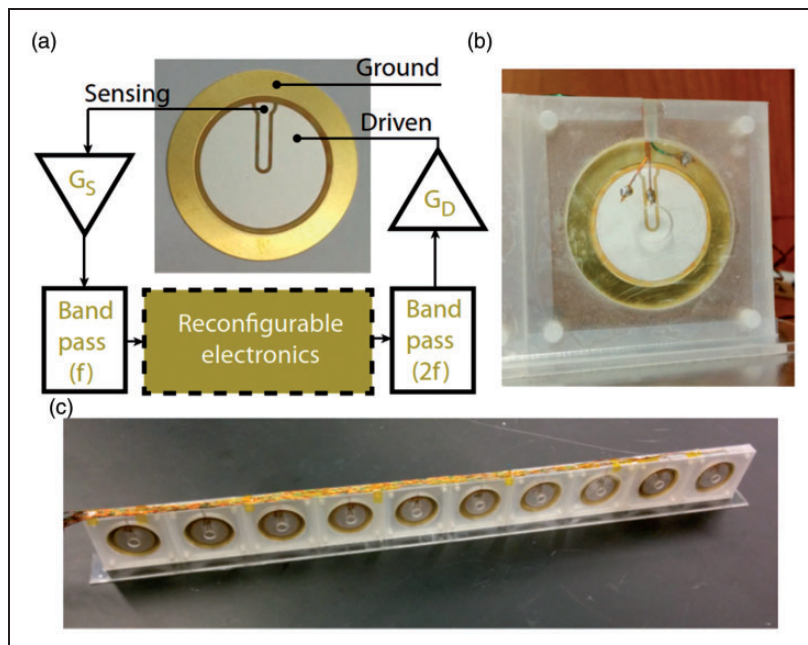


Figure 8. (a) The reconfigurable metamaterial unit cell; (b) photograph of a fabricated unit cell; (c) metamaterial slab consisting of ten cells.²²

properties, which could reach a wider range of electromagnetic bandwidth. Furthermore, in the promising area of smart metamaterials, it is rather common to employ an external magnetic/electric field to alter the behavior of the metamaterial.

Mendhe and Kosta²⁴ studied the properties of such metamaterials and their applications. The permittivity and permeability in metamaterials could be negative or positive; therefore, they were divided into four classes. The different classes of electromagnetic metamaterials have been shown in Figure 11.

The exceptional properties of electromagnetic metamaterials, such as the negative refractive index, have attracted much attention. These materials are artificially made and on scales smaller than the wavelength. Contrary to ordinary magnetic metamaterials designed for working at resonant frequencies, Magnus et al.²⁵ considered magnetic metamaterial

consisted of superconducting plates for working at zero frequency. They calculated the effective permeability of the structure and showed that it matches with the dramatic results. The view of these plates and the magnetic field between them is shown in Figure 12.

Due to the need for wireless communications in the military, industry, and environment, various researches are devoted to the advancing electromagnetic metamaterials. The presence of complex structures and weak intermediates in conventional wave-based electromagnetic techniques has made them inoperable, and magnetic induction has been used in their stead. On the other hand, due to the small size of the antenna in communications based on magnetic induction, the communication range is low. Magnetic induction has been thus used to resolve this problem. Based on the theoretical results, the

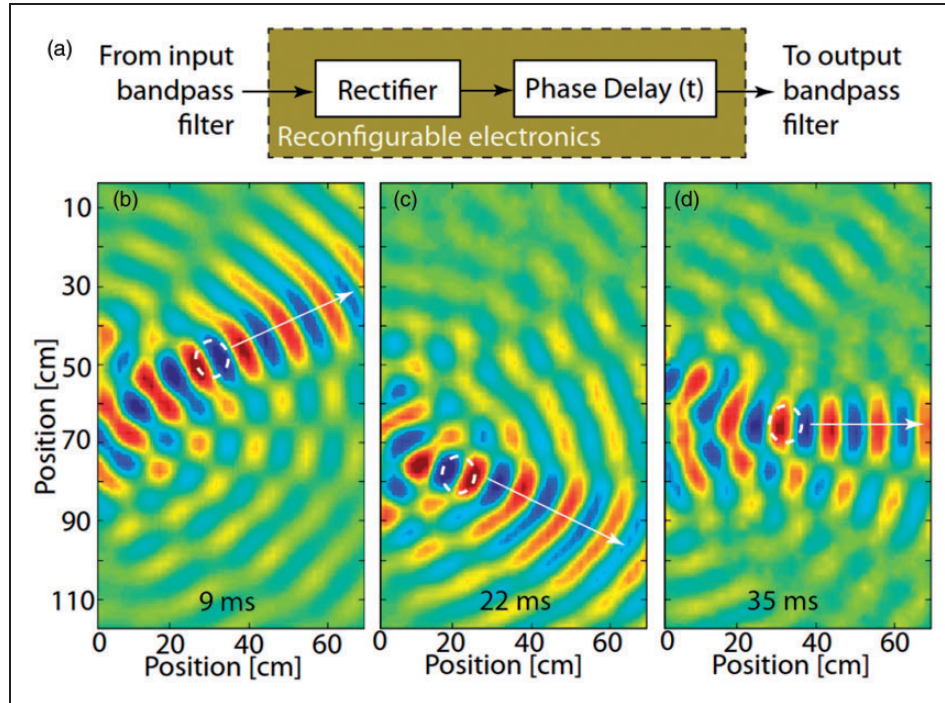


Figure 9. Metamaterial lens configured to multiplex functionality: (a) diagram of the reconfigurable electronics showing two-phase delay lines that implement the two desired behaviors; (b) the first functionality is that of a focusing lens identical; (c) metamaterial configured to behave like a beam steering device; (d) metamaterial configured to behave as a focusing lens and beam steering device.²²

increased magnetic induction dramatically increased the communication speed of data and amplitude; however, it was not the case in practical situations. An ideal spherical model is displayed in Figure 13.

Guo et al.²⁶ designed a practical specimen's geometric structure using an array of spherical coils and found the optimal settings. Metamaterial-enhanced magnetic induction design challenges were the construction of spherical metamaterials, control of the useful parameters, and the need for more considerable transmission distances than antenna size. Experiments showed that the performance could be improved by expanding the number of shell layers to engage more metamaterial elements, reducing the resistance of the coil, or increasing its rotations. Figure 14 shows a metamaterial coil and a single cell.

Boyat and Hafner²⁷ designed a quasi-static metamaterial to shape the magnetic field's flow while protecting it. The possibility of creating heterogeneity using metamaterials had improved their performance compared to traditional protective materials. Creating additional heterogeneity in metamaterials also made them perform much better. The different methods of protecting the magnetic field for metamaterials are illustrated in Figure 15. Magnetic field protection in materials with high permeability was based on guiding or trapping the magnetic field and in

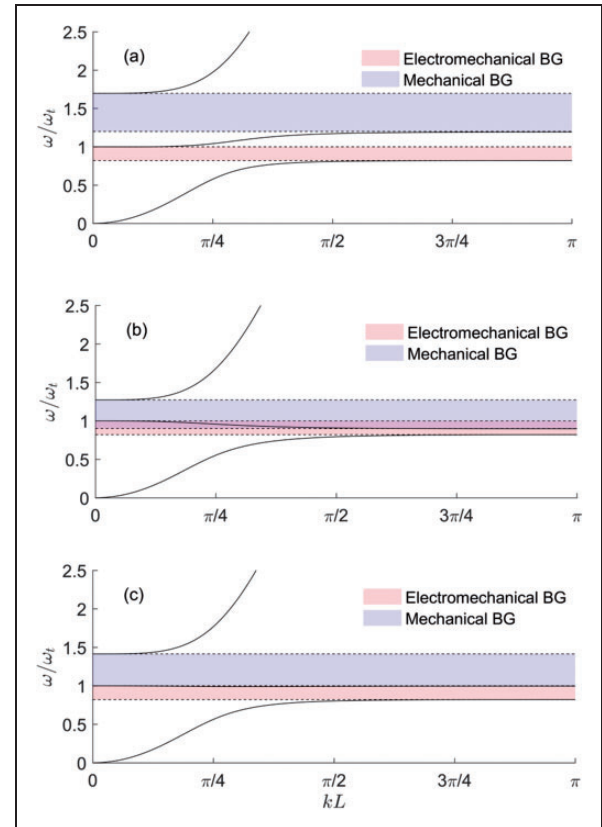


Figure 10. Dispersion curves from plane wave expansion.²³

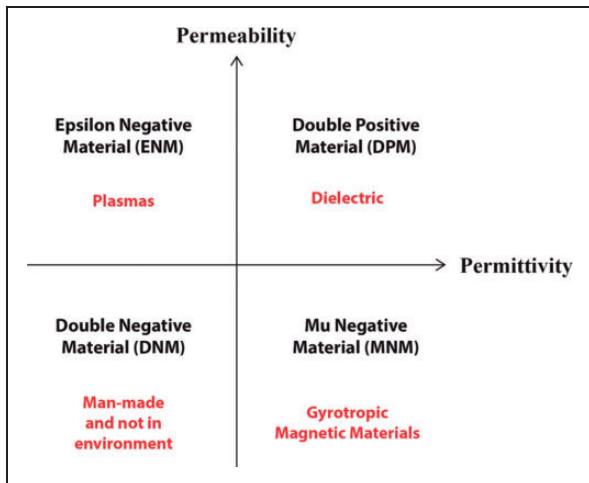


Figure 11. Four classes of electromagnetic metamaterials.

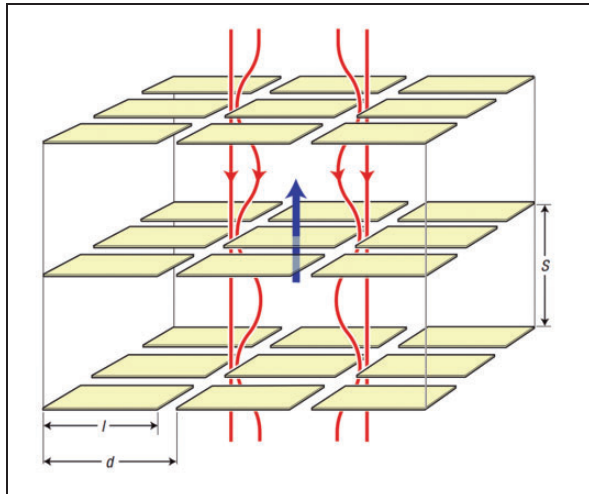


Figure 12. Superconducting plates and the magnetic field between them.²⁵

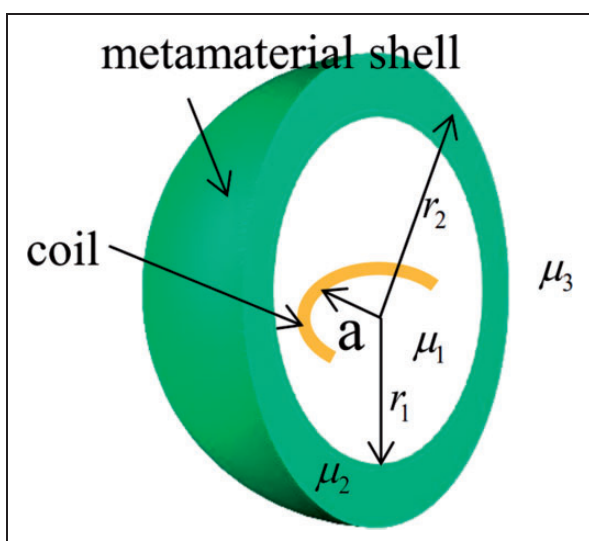


Figure 13. Increased magnetic induction model.²⁶

materials with low permeability was done by repelling the magnetic field. Magnetic field protection was also improved when a non-isotropic material with different permeability coefficients in different directions was used.

Magnetic resonance imaging is the primary technique for achieving anatomical images in the human body. In laboratory studies, animals were used instead of humans. Ali et al.²⁸ designed and analyzed the magnetic metamaterial hat that enhancing the signal-to-noise ratio and also improved the radio frequency rotation's symmetry around its axis. The schematic view of this experiment is shown in Figure 16. Finally, they experimented on the brain of a mouse and optimized the image quality by changing the position of the mouse's head in the presence or absence of a magnetic metamaterial hat.

Abirami et al.²⁹ reviewed the theory of magnetic left-handed materials, which could be a composite. The artificial structure of this type of metamaterial included split-ring resonators with wires inside them. The refractive index of these metamaterials was negative, and as a result, the phase and group velocities of the electromagnetic wave had opposite signs. The negative refractive index feature has led to metamaterials in watchmaking devices, lasers, ultrasonic fields, optical communication, and aerospace applications. They examined the changes in the refractive index's real and imaginary parts and the resonant frequency by changing the magnetic field. They showed that as the magnetic field increased, the resonant frequency also increased. The composite metamaterial system is illustrated in Figure 17.

Chiral metamaterials

In its essence, the main feature of chirality is breaking mirror symmetry. Many objects, including the human body and man-made products, are an example of chirality in nature. A piece of material is called "chiral" if it cannot match its mirror image by rotating or transmitting the image. Chiral metamaterials behave differently from their mirror counterparts. Lightweight mechanical chiral metamaterials are frequently used as vibration attenuation and energy harvesting due to these unique properties. The structure of chiral metamaterials provides lightweight construction with a flexible topological adaptation that makes it suitable for ultra-sensitive biosensors. Chiral metamaterials offer a very convenient method for actively regulating the light field through external devices—an essential attribute in nanophotonics. However, the chiral response of generally flat metamaterials severely limits their application. Therefore, designing a system with a sizeable rotational color scheme is very important. In 2019, Chen et al.³⁰ introduced a new type of chiral metamaterial based on plasmonic, bilayer, and rib-shaped nanoparticles with 60°

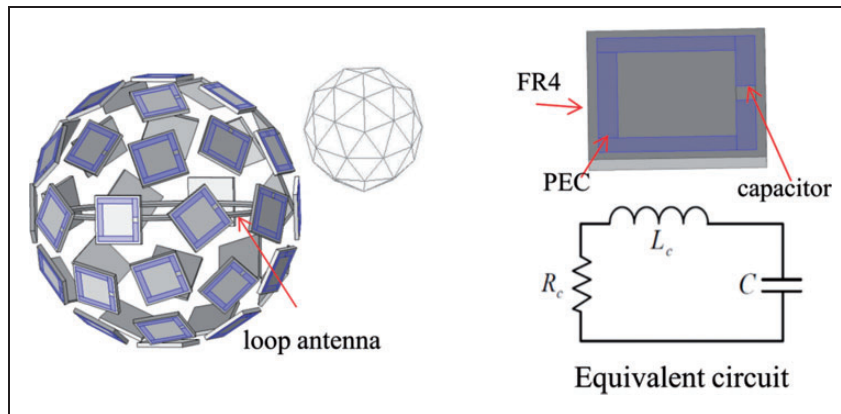


Figure 14. Metamaterial coil and a corresponding unit.²⁶

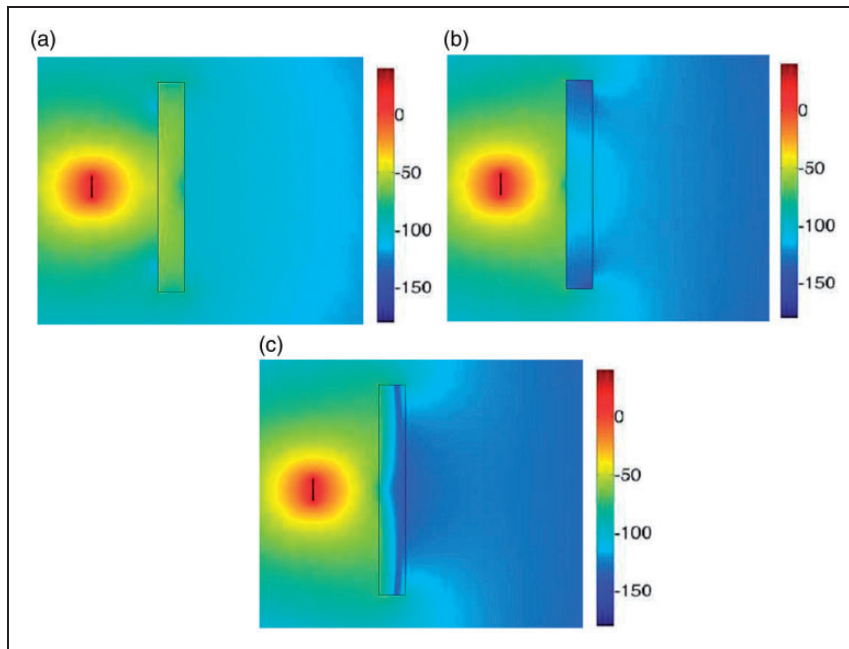


Figure 15. Different methods of magnetic field protection in metamaterials.²⁷

rotational layers to trap atoms. In their study, an optical metamaterial with strong chirality in a two-layered plasmonic structure was investigated. Figure 18 shows the schema of this structure. The single cell of the chiral plasmonic structure was composed of two thin silver layers that had a rotating shape and rotated at an angle of 60° to each other. The second layer of the film grew on the silica bed and was separated by a thin layer of silica from the first layer. This type of atom-trapping method would be of great importance in quantum and nanophotonic information processing.

There are various biosensor structures based on metamaterials. However, biosensors based on chiral metamaterials are sufficiently investigated. Sabah et al.³¹ designed a microwave biosensor based on a chiral metamaterial. The biosensor was used for discovering pig biological tissues. Structures based on

rhombus shape resonator in microwave frequency regime had been numerically analyzed. The results were in good agreement, indicating that the proposed biosensor had many applications in medical technologies. Biosensors based on chiral metamaterials were designed and tested for large, small, and almost zero chiral values. In the first step, the proposed chiral metamaterial was based on rhombic resonators designed for large chiral scales. The proposed model included rhombus shape resonators in the upper and lower layers. A dielectric substrate existed in the middle layer too. Figure 19 shows the proposed model with large chiral values.

In the second step, the proposed chiral metamaterial was based on rhombus shape resonators designed for small chiral scales. The proposed model included rhombus shape resonators in the upper layers and dielectric substrates in the lower layers. The second

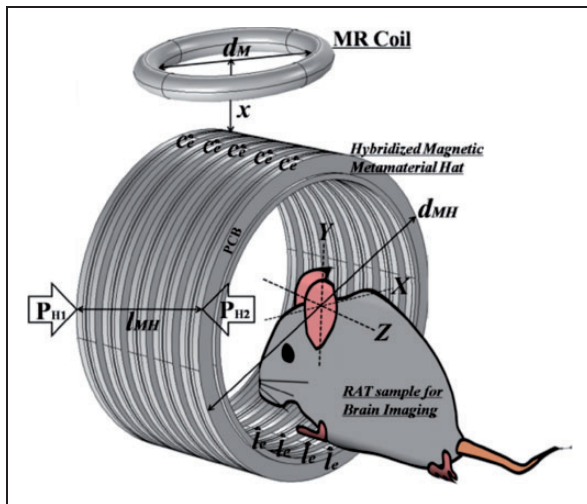


Figure 16. Magnetic resonance imaging in the presence of a magnetic metamaterial hat.²⁸

proposed model with small chiral values is shown in Figure 20.

In the third step, the proposed chiral metamaterial was based on rhombus shape resonators designed for zero chiral scales. The proposed model included rhombus shape resonators in the upper layers and dielectric substrates in the lower layers. This proposed model with zero chiral values is displayed in Figure 21.

The influence of the variations of bone marrow temperature on the parameters of frequency resonance, transmission, chirality, and reflectance of different structures was tested, and the sensitivity of the mentioned parameters to temperature changes was investigated. The frequency of reflectance changes for different chiral values and at different temperatures were investigated and displayed in Figures 22 to 24. For structures with high chiral

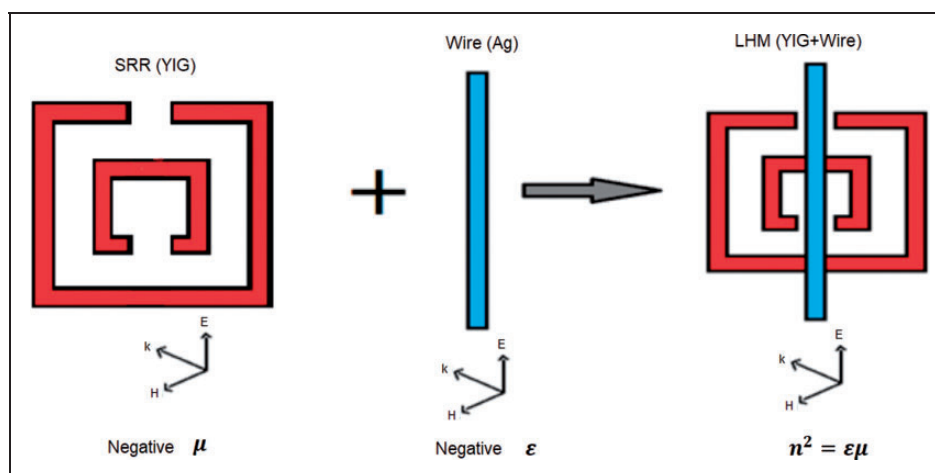


Figure 17. Composite metamaterial system.²⁹

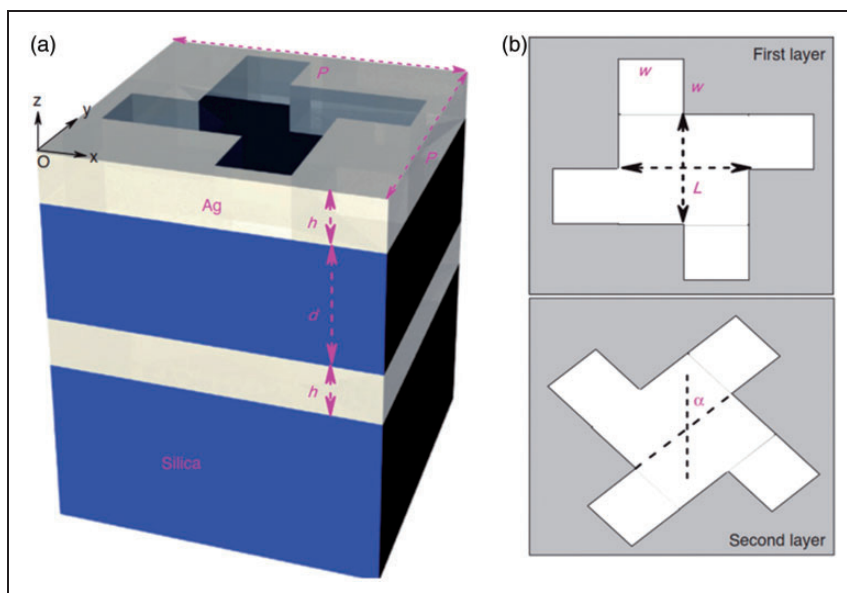


Figure 18. Schematic of the chiral metamaterial structure and its top view.³⁰

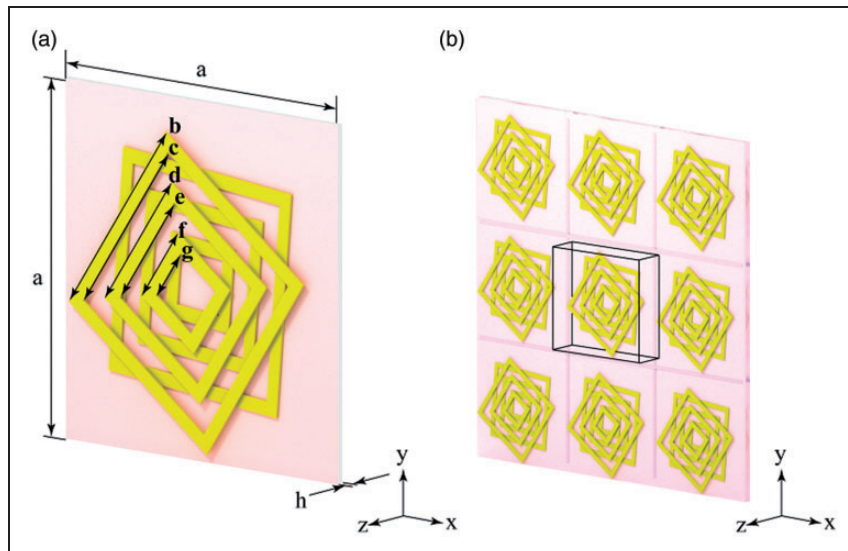


Figure 19. The proposed model with large chiral values.³¹

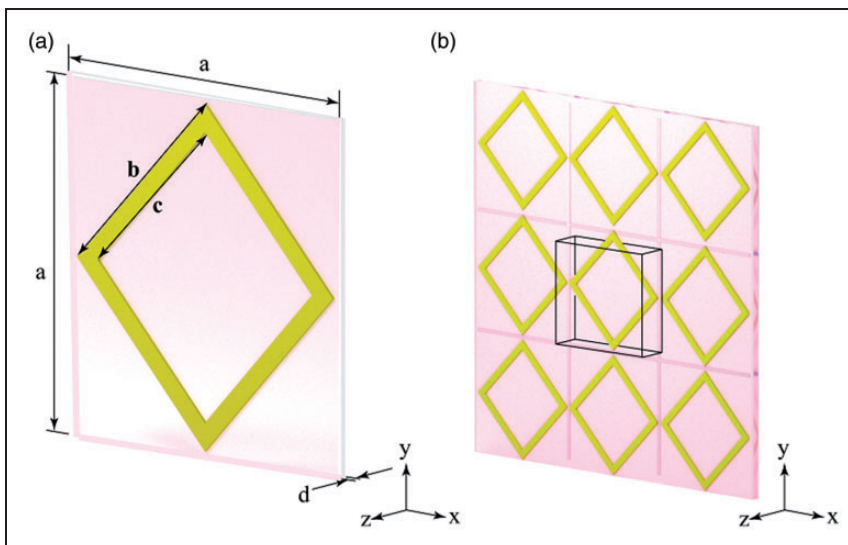


Figure 20. The proposed model with small chiral values.³¹

values, the proposed model did not show accurate reflections in the frequency range of 6.5–8 Hz and 11–15 Hz, but in the range of 8–11 Hz, it exhibited a good reflection coefficient. With increasing bone marrow temperature, the reflection coefficient was transferred to the higher values. For structures with small chiral values, the proposed model did not have a good reflection coefficient in the frequency range of 9–15 Hz but had a good reflection coefficient in the frequency range of 6–9 Hz. In this case, as the bone marrow temperature rose, the frequencies associated with the minimum and maximum reflections were shifted to the left. The proposed model did not show a useful review in the specified frequency range for structures with chiral values close to zero. However, the electromagnetic wave reflected linearly in the frequency range of 14–16 Hz.

The results showed that these parameters were susceptible to temperature changes, and the temperature changes could be identified with high accuracy.

One of the critical applications of engineering elastic metamaterials is the attenuation of low-frequency vibrations due to the unusual bandwidth behavior at low frequencies. However, some of the available elastic metamaterials' bandwidth is narrow and causes their practical engineering applications to be limited. Zhu et al.³² introduced a grid-elastic metamaterial with multiple local resonators to attenuate broadband vibrations without altering the bearing load. In the first step, a theoretical beam model was proposed for achieving the bonding behavior of an elastic metamaterial beam with multiple resonators. Finally, an elastic metamaterial beam was made, and laboratory tests were performed. The experimental results were

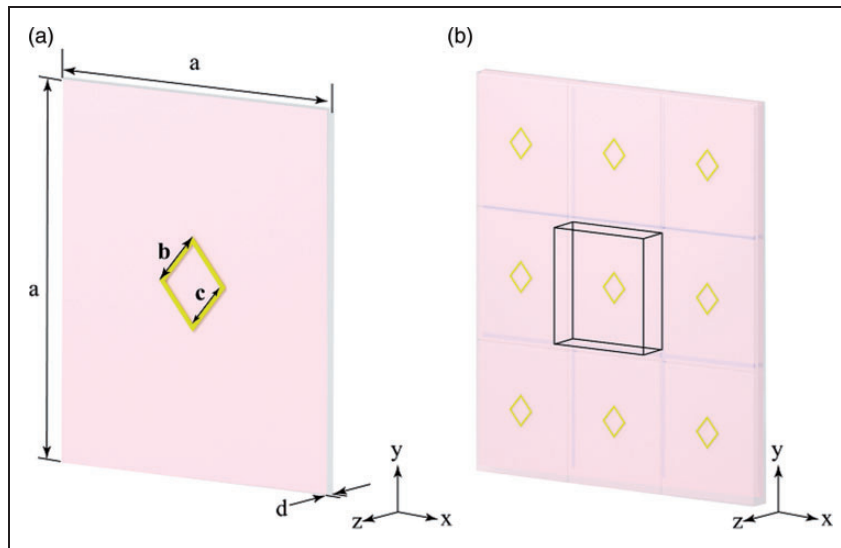


Figure 21. The proposed model with zero chiral values.³¹

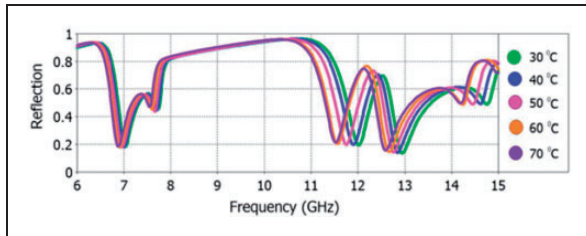


Figure 22. Frequency reflectance changes for biosensor with high chirality at different temperatures.³¹

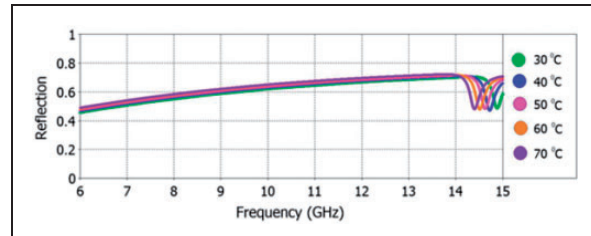


Figure 24. Frequency reflectance changes for biosensor with chirality close to zero at different temperatures.³¹

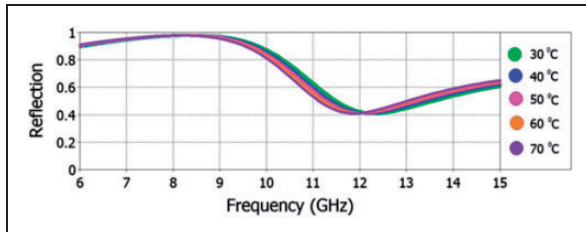


Figure 23. Frequency reflectance changes for biosensor with small chirality at different temperatures.³¹

compared with the theoretical predictions. In the first stage, the elastic metamaterial beam was made of aluminum. Zhu et al.³² used a metamaterial beam and a single cell, as depicted in Figure 25. The beam structure was alternately sandwiched to the beam frame, and the end of each ligament was rigidly attached to the edge. The local resonators made of rubber are connected to the steel and tungsten cylinders. The elastic metamaterial beam was fixed on one side and stimulated by a vibrator near the fixed end. An amplifier powered the vibrator. When the vibrator generated the disturbance excitation signal with a bandwidth of 0–1000 Hz, the elastic metamaterial beam's response was recorded by the accelerometer attached

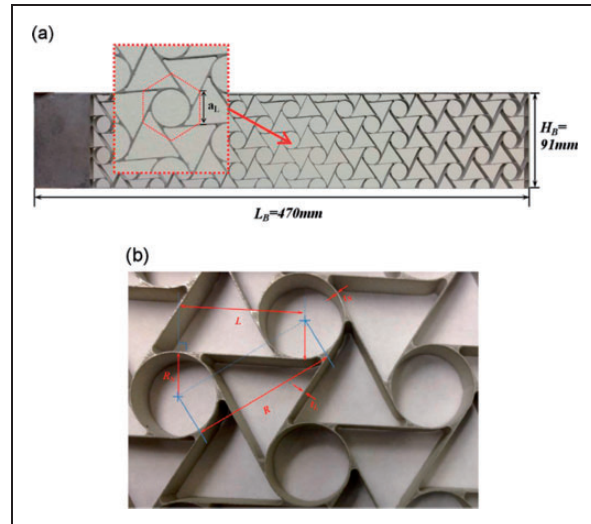


Figure 25. A metamaterial beam and a single cell.³²

to the other end of the metamaterial beam. The signal analyzer recorded both input and output signals. A laptop that used data logging software to perform preprocessing operations was used. The power sensor's ratio of the output signal to the accelerometer's input signal was called the frequency response curve.

The experiment was performed without resonators' presence, and frequency response curves were obtained in the first step. In the next step, frequency response curves were recorded with a different number of resonators. This paper proposed elastic metamaterial beams with multiple resonators to suppress broadband vibrations by generating a specific bandwidth for each resonator.

Wu et al.³³ presented an interesting review article in which they investigated the two-dimensional and three-dimensional chiral metamaterials properties and applications. In the first step, they introduced the auxetics as the materials with a negative Poisson ratio deformed perpendicular to the applied load and then examined the chiral metamaterials as an auxetics class. A material was called chiral if it could not match its mirror image by rotation and translation. The different chiral metamaterials including chiral, anti-chiral, and meta-chiral are depicted in Figure 26.

Many articles about examining the deformation mechanism of two-dimensional and three-dimensional chiral metamaterials were studied in the next step. The strain energy method or unit cell balance could be used to investigate the deformation mechanism. By looking at the next part of that article, it was found that changing the ligament's flexural shape, rotating the nodes, the properties of tunable bandgap, vibration attenuation, energy absorption, and zero coefficient of thermal expansion could be created in the chiral metamaterials. In the end, applications of chiral metamaterials in different fields such

as biomedicine, aerospace, and smart materials were elaborated.

Metamaterial absorber

The first metamaterial absorber was composed of a dielectric layer and two metal layers and was made by Gangwar and Gangwar³⁴ in 2008. The absorber at 22,984 (Hz) showed 22% absorption, while Landy achieved a 44% absorption in his experiments.³⁵ False errors were the origins of this discrepancy. Figure 27 depicts this absorber and its single cell.

Hossain et al.³⁶ designed a perfect metamaterial absorber consisting of two metal layers separated by a dielectric substrate of the gallium arsenide to extract solar energy. The solar cells of this adsorbent could increase the efficiency of the system by intensifying the solar electromagnetic wave. The desired adsorbent metamaterial in the electric and transverse magnetic modes has reached the peak of adsorption. The results showed that changing the thickness of the different absorbent layers, the polarization angle, and the dimensions and shape of the resonators could change the absorption rate. Figure 28 shows the designed absorbent and figure 29 represents the variation of the absorption rate in terms of frequency for patches with different shapes (hexagonal, octagonal, pentagonal, and circular) that were developed in their research. The results exhibited that the hexagonal shape was more suitable for solar energy harvesting due to its high absorption rate.

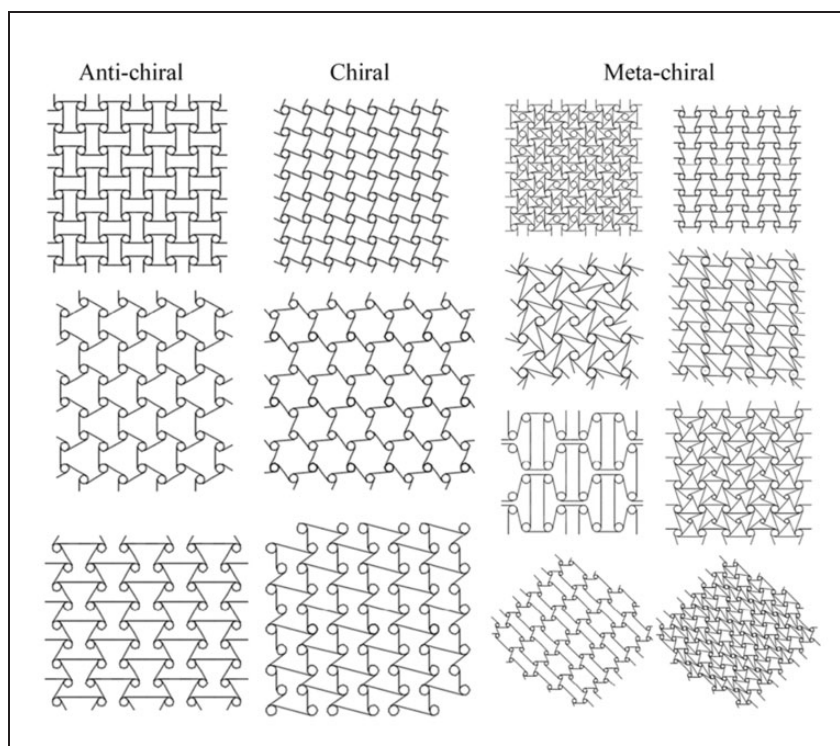


Figure 26. Types of two-dimensional chiral metamaterials.³³

Tran and Phuong³⁷ designed a perfect metamaterial absorber consisting of two dielectric layers for adsorption on the k-band. They optimized the structure's dimensions and examined the effect of the structure's dimensions and the distance between the two layers on the absorption rate. The experimental and numerical results showed the high dependence of the structure performance on its dimensions. Figure 30 illustrates the corresponding two-layer structure.

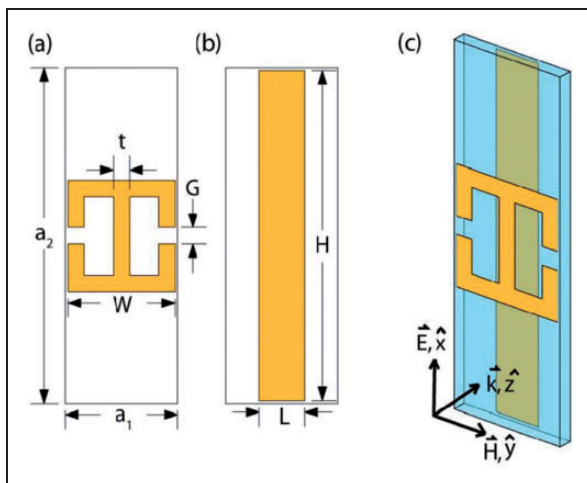


Figure 27. Metamaterial absorber and its unit cell.³⁴

The experimental method was used to confirm the simulation results, and good agreement was observed. The difference in the frequency and absorption could also be due to model defects, inaccuracies in permittivity, and measurement errors. Figure 31 shows the absorption rate curve versus frequency for the experimental and simulated states.

Xie et al.³⁸ designed a water metamaterial absorber to absorb broadband and low dependence on liquid phase temperature. The proposed metamaterial absorber was low cost, high absorption, and useful in electromagnetic energy extraction. The metamaterial absorber and its layers have been depicted in Figure 32.

They considered different modes for this metamaterial absorber demonstrated that the optimal absorbent could achieve an absorptivity of about 90% over a wide frequency range. The absorption rate for all the absorbent layers was composed of water, and no hole was 35–40%. When the absorbent lacked water, the absorption rate was reduced to 20–40%. The variation of the absorptivity in terms of frequency for different modes was investigated and is shown in Figure 33.

Nonlinear metamaterials

The problem of nonlinear metamaterials has received relatively little attention. Gao et al.³⁹ presented a nonlinear metamaterial model with an effective negative

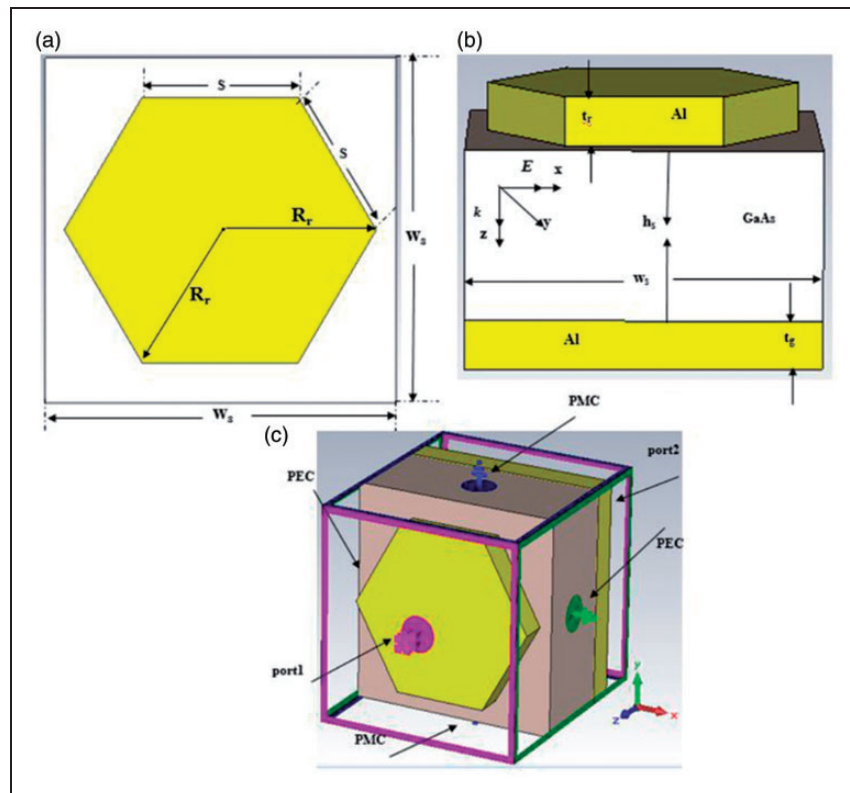


Figure 28. Perfect metamaterial absorber and its unit cell.³⁵

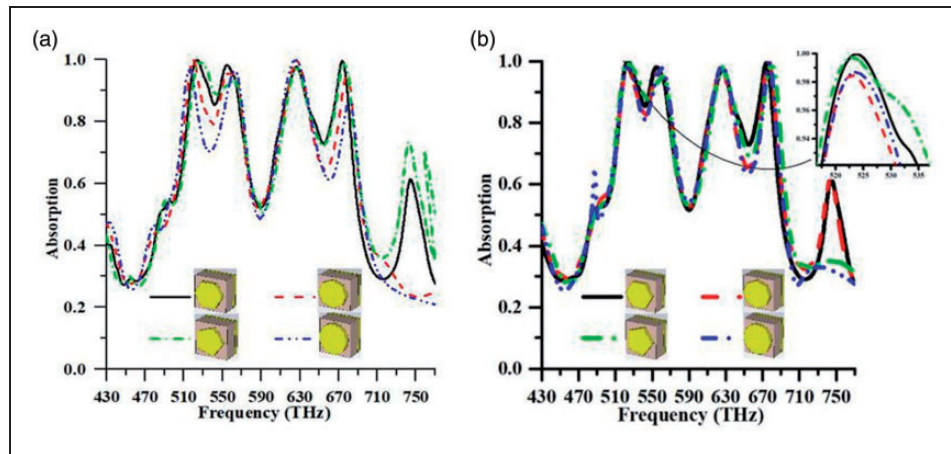


Figure 29. Variation of the absorption rate in terms of frequency for patches with different shapes (a) the different effective area and (b) the same effective area.³⁵

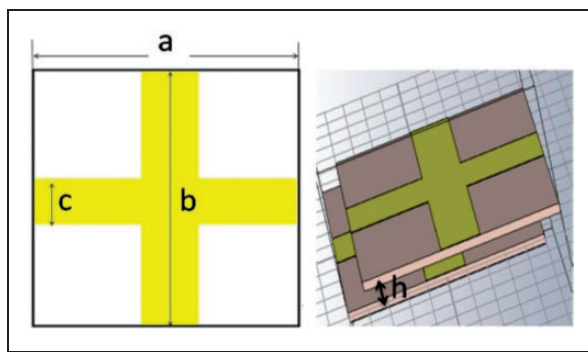


Figure 30. Metamaterial absorber with optimal dimensions.³⁶

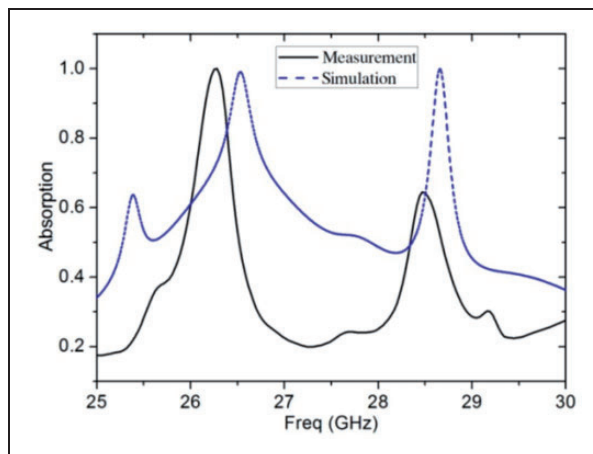


Figure 31. Absorption rate versus frequency for the experimental and simulated states of the metamaterial absorber.³⁶

mass. They used Poincare's theory to obtain the wave propagation curve. Then the frequency position of the start and cut frequencies were determined. In this paper, it was shown that there was an effective positive mass in the nonlinear bandgap. Finally, the numerical solution proved the results of the

theoretical analysis. Each metamaterial element used in this study was a shell with a nonlinear spring-mass attached on both sides. Each element was connected to the other element by a linear spring.

Cveticanin and Zukovic⁴⁰ designed a nonlinear metamaterial subsystem. The nonlinear model absorbed acoustic waves in a wide frequency range. This subsystem consisted of two concentrated masses connected by a nonlinear spring, and the whole system was excited by the elliptic Jacobian function. The corresponding system has been shown in Figure 34.

The system's mathematical model was transformed into two coupled differential equations of Duffing type—assuming cubic stiffness nonlinearity for the springs. Modification of the equations decoupled the system into two linear and nonlinear differential equations. They solved the Duffing equation by excitation determined in the form of the elliptic Jacobian function. The movement of the masses under the system was alternating around a medium range. The motion of the first mass must be much less than the second one. Excitation with some parameters resulted in the creation of a high attenuation dynamic system, although the range of motion was not zero for this case but was small for a wide range of excitation frequencies. The results showed that the frequency bandwidth for a nonlinear system was much larger than the linear system. In the nonlinear system, when the mass ratio is negative, the frequencies corresponding to the negative mass ratio are in the stop-band. The shape of the modes corresponding to these frequencies is known as the optical mode.

Gao et al.³⁹ numerically proved that the structure with decent nonlinearity would broaden wave attenuation frequency regions compared with the corresponding linear counterparts. Moreover, it produced higher harmonic wave dissipative triatomic lattice using narrowband excitations. They proposed the nonlinear triatomic mass-spring lattice and

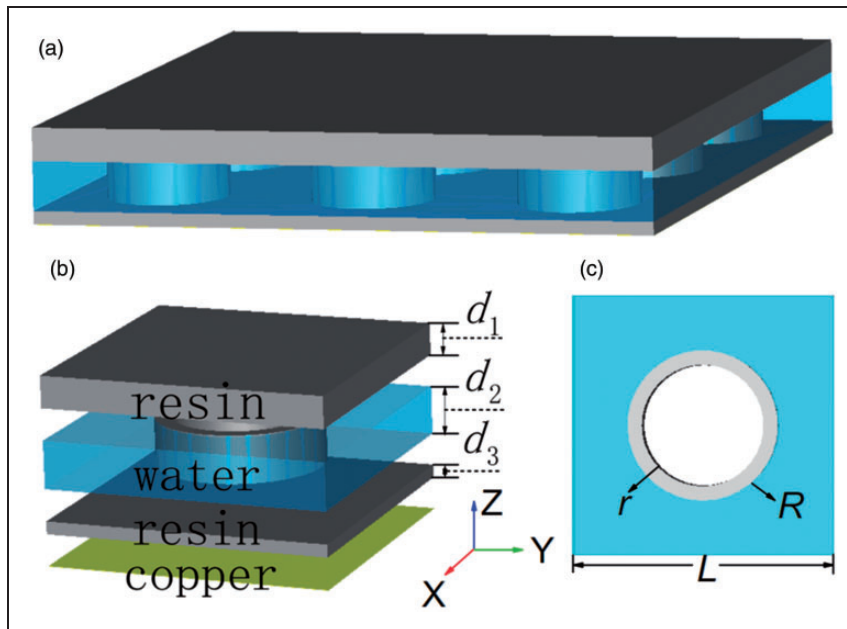


Figure 32. (a) Water metamaterial absorber, (b) view layer by layer, and (c) top view water layer.³⁷

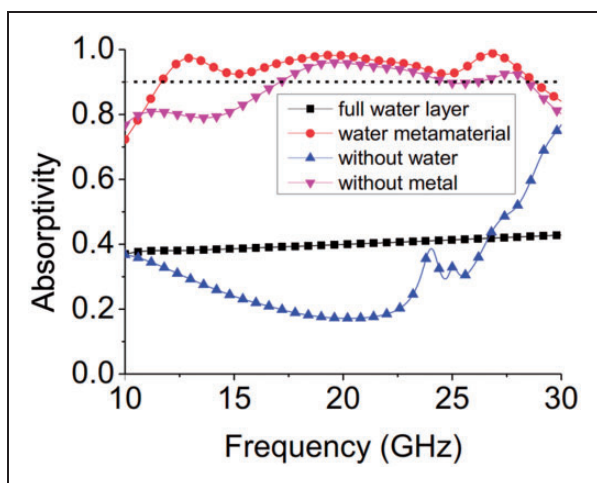


Figure 33. The variation of the absorption rate in terms of frequency in different modes.³⁷

determined proper nonlinear and damping parameters to enhance the attenuation frequency of the region. The proposed metamaterial capacity was examined by a time-domain analysis conducted using the fourth-order Runge–Kutta method for calculating the transient displacement fields within the 15-unit cell lattice. Finally, they showed that increasing the damping coefficient caused the chaotic behavior and frequency up-conversion to be weak, and consequently, the damping coefficient chiefly governed the amplitudes of harmonic waves generated in the nonlinear media. Suitable combining nonlinearity and the material damping completely suppressed the transmitted wave amplitudes. The amplitude decline of the reflected signal showed that the nonlinear structure absorbs more incident energy than the linear one.

Khajehtourian and Hussein⁴¹ investigated wave propagation in nonlinear metamaterials. The model was one-dimensional and elastic and included a narrow bar with intermittent local resonators. Deformation in the bar was large and elastic; therefore, the model was nonlinear, and the system behavior was evaluated by local resonator dynamics. They approximated a dispersion relation for this model and predicted the bandwidth parameters analytically. Then the effect of nonlinearity on the bandgap parameters was studied. The parameters were bandgap size and bandgap location. The schematic of the one-dimensional metamaterial rod used by them is shown in Figure 35.

This paper presented an analytical formula for calculating one-dimensional elastic metamaterial dispersion curves with the local resonance property. The model was considered to be a uniform, narrow bar with alternating spring-mass resonators. The nonlinear effect was included precisely on the base surface of the rod. They applied the transfer matrix method to the single-cell and approximated a dispersion relation for the one-dimensional metamaterial set. The higher-order strain expressions were removed to approximate the transfer matrix method. Many systems with different resonance parameters were analyzed to investigate the nonlinear effects on bandgap behavior. According to the results, the location and size of the bandgap changes increased with increasing wave amplitude. Moreover, the bandgap property (Bragg scattering versus hybrid local resonance) could change in some cases, leading to two types of bandgap and forms a composite bandgap. If elastic wave propagation was linear, the error increases with increasing wave amplitude.

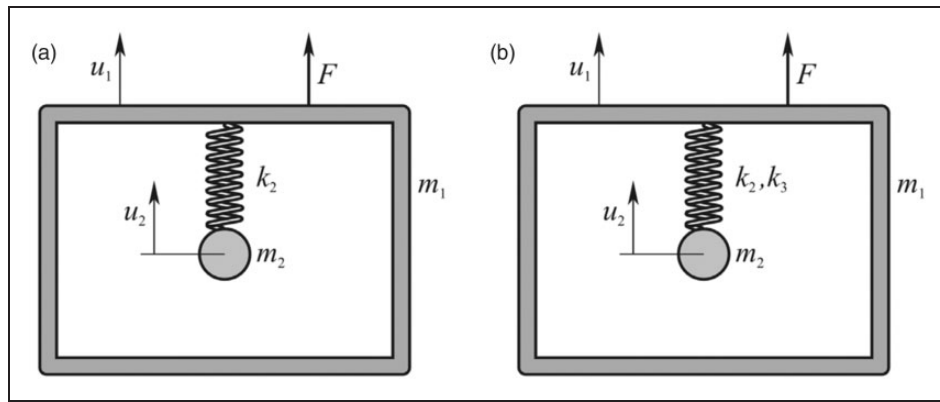


Figure 34. Linear and nonlinear model of the system.³⁹

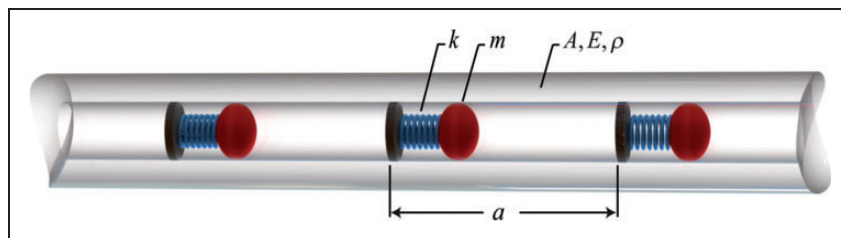


Figure 35. Schematic of one-dimensional metamaterial elastic rod.⁴⁰

Xia et al.⁴² investigated the nonlinear metamaterials. This study examined the increase of bandwidth depending on amplitude in metamaterial vibrations with bi-stabilized connections. For the system's mathematical analysis, each cell consisted of a combination of a significant mass and a related mass connected by a nonlinear spring. The cells set were related to the adjacent set by a linear spring. By deriving the equations at $2N$ degrees of freedom (N number of significant objects) and solving the harmonic method, two equilibrium points for each connected mass were obtained by assuming that the linear term of nonlinear spring was negative. Such a structure was called a bi-structure. Fourier coefficients and the Newton–Raphson method were used for periodic excitation, and the Runge–Kutta method was used for non-periodic excitation. To validate, the system results with 10 degrees of freedom were calculated numerically and compared with the experimental results. In this study, the level of force required to escape energy wells from the point-of-contact bias was determined and calculated. In practical calculations, the bandwidth of the domain was evaluated.

The metastructure was designed as a cantilever beam with magnetic beams as bi-stable masses in the joints. These joints were intended as a cantilever steel beam with a concentric mass at the end. These masses were two cubic magnets with hollow holes in the middle of each. Two magnets were fixed at the bottom of the beam to determine the bi-stable position. The structures were subjected to an incremental frequency of 8–20 Hz and a reduced frequency of

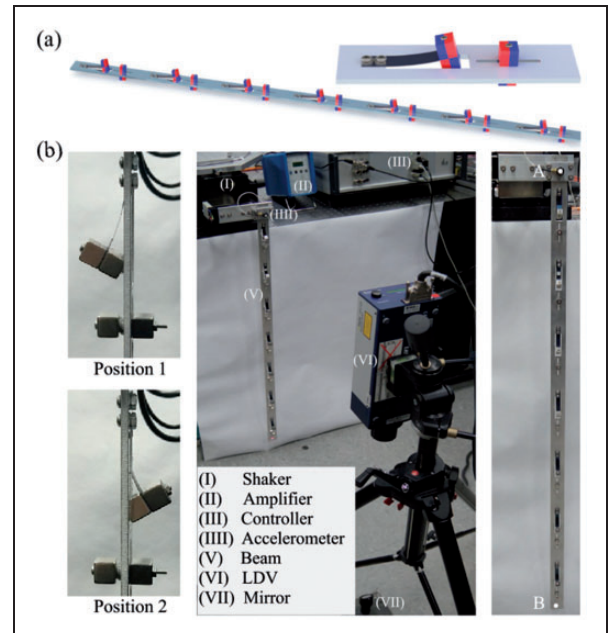


Figure 36. Mass and connection mass and experimental test setup.⁴¹

20–8 Hz at a rate of 0.25 Hz/min. The structure could be positioned in bi-stable wells by varying the fixed and removable magnets (Figure 36). The results showed that the bandwidth in nonlinear vibrations was broader than that of linear vibrations. The proposed unit cells allowed flexibility in the potential wells of the bistable attachments by varying the

distance between pieces of magnets. As seen in Figure 37, the base vibration rise transformed the linear resonance into nonlinear softening behavior, and thereupon interwell oscillations and chaos were observed, which dramatically attenuated the vibration within the produced bandgap.

Terahertz metamaterials

Asgari et al.⁴³ introduced a dynamically tunable microelectromechanical terahertz adsorbent. This metamaterial adsorbent included U-shaped ring resonators and shear wire resonators. The three-dimensional schematic of the single cell, in two states of on and off, is shown in Figure 38. The top layer of this adsorbent was made of aluminum, the next layer was aluminum oxide, and the bottom layer was polyamide. In the first step, when the voltage across all layers exceeded 24 V, two resonators contacted the substrate and caused the state of on to be created. When the corresponding voltage was canceled, the two resonators were released and returned to the original condition by the storage power. The direction of the electrostatic forces and the storage forces was opposite to each other. The modeling approach was straightforward with the use of an

analogous circuit model. Numerical analysis was carried out by using a finite integral method. A comparable circuit model was used to illustrate the effects of the numerical process. The electrical control of the terahertz metamaterial absorber has provided conditions for using photonic integrated circuits, devices, and terahertz circuits.

Acoustic metamaterials

An AM is an artificial structure designed to steer, direct, and manipulate acoustoelastic waves with extraordinary properties unavailable in nature. Control of acoustic waves is possible by negative sufficient mass density and effective bulk modulus based on resonance mechanisms as well as exceptional scattering properties. This wealth of metamaterial parameters is used in a wide variety of applications from noise reduction to acoustic cloaks.

Hu et al.⁴⁴ investigated a modified AM system. The system consisted of local resonators that were connected by linear springs. The designed acoustic model had three bandages that could suppress broadband vibrations. Initially, the number of grids was considered infinite, and the first band structure of the modified AM was calculated using Bloch

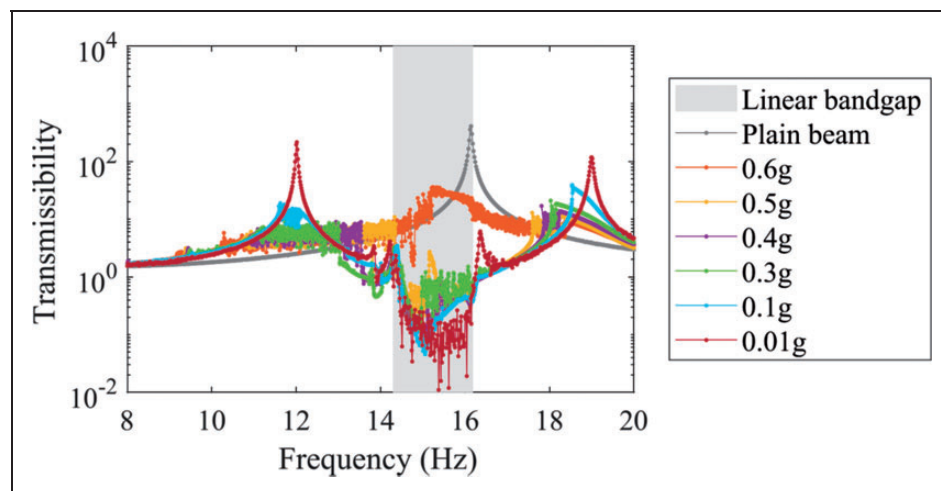


Figure 37. A reinforced nonlinear-base structure shows a dramatic enhancement of the attenuation bandwidth than the plain beam.⁴¹

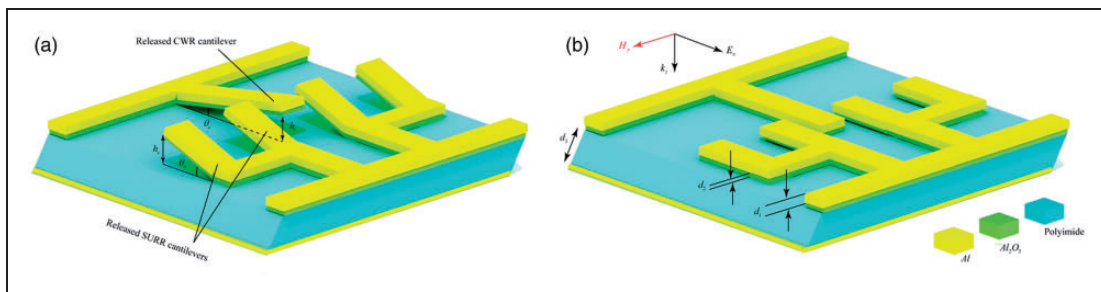


Figure 38. Microelectromechanical terahertz metamaterial absorber.⁴²

theory. The effect of spring and mass parameters on the bandgap behavior of the modified AM was investigated by using a dimensionless parametric relationship. According to the calculations, the modified AM band structure had three bandgaps. By optimizing the dimensionless parameters, the maximum bandwidth was reachable in the low-frequency range, and a credible model with a finite network number could be achieved. After calculating the transmittance of the conventional and modified model, it was found that the bandwidths and the vibration attenuation behavior of the system that using Bloch theory for the model with an infinite number of networks were in good agreement with the results of the transmittance. After calculating the time response, it was shown that the modified metamaterial model performed better than the conventional model. Figure 39(a) and (b) shows a typical and modified sample with an infinite number of grids. The modified metamaterial system with a finite number of grids is also shown in Figure 39(c).

In Figure 40, bandgaps of the conventional and modified metamaterial structures are compared. The modified metamaterial sets up three expanding bandgaps, whereas the conventional metamaterial system formed just one narrow bandgap.

The displacement of the last masses of these aforementioned metamaterial systems was compared and shown in Figure 41. The vibration amplitudes in both the conventional and the modified metamaterial systems decreased rapidly at the bandgap frequency. Subsequently, the vibration amplitude rebounded as the frequency traveled from the bandgap bound. In the modified metamaterial structure, the vibration amplitude remained close to zero for a much longer time than in other forms.

Ebrahimi-Nejad and Kheybari⁴⁵ designed a local resonance metamaterial adsorbent in the cubic and the rectangular cube shape, consisting of cells with square and honeycomb shape. For validating the numerically obtained model, a box containing a

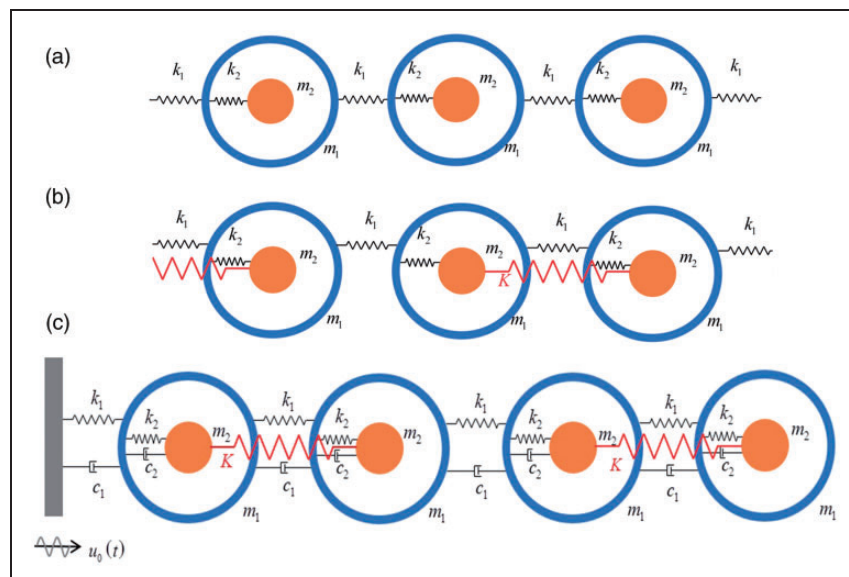


Figure 39. Three kinds of network models of metamaterial system.⁴³

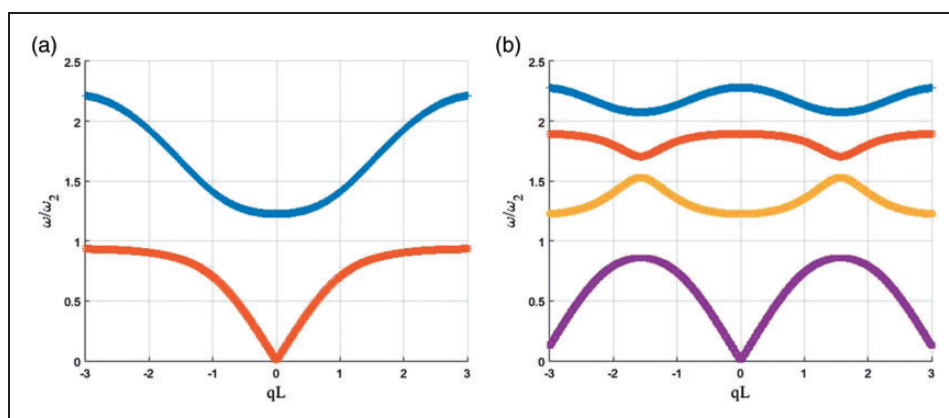


Figure 40. Band structures of (a) conventional metamaterials and (b) modified metamaterials.⁴³

metamaterial acoustic panel was fabricated. Then, AM models were simulated. The structures were considered cubic and rectangular cubic, and the single cells were simulated as square and honeycomb. In this study, the performance of different AMs in a specific frequency range was analyzed and compared. The metamaterial panels were made of several plates, each with spring and mass elements. The panels were the cube and rectangular cube with 64 and 30 square and honeycomb unit cells. Honeycomb unit cells had two spring and mass resonance elements, and each square unit cell had a resonance element. The single cells were coated with plexiglass and were equivalent to the spring and mass resonance elements in the model structure. The result of modifying the number and type of the unit cell, integrating two adsorbents into one single cell, cubic and rectangular cubic structures were modeled in five ways to investigate various acoustic behavior of metamaterial models. The first natural frequency of AM unit cells was calculated, and after comparing the results with the experimental method, good agreement was observed. The mechanical properties of a single cell were measured using an experimental method, and the force-displacement curve was extracted. The experimental test for measuring mechanical properties used in the above research is shown in Figure 42.

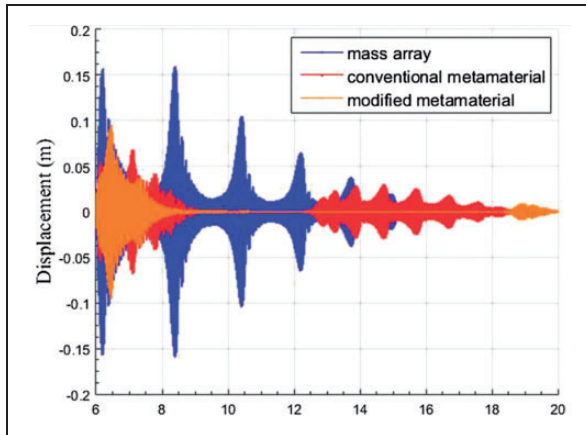


Figure 41. Displacement responses of various systems due to broadband chirp excitation.⁴³

To obtain the stopping frequency of AMs and investigate their alternating band behavior, square metamaterial plates were modeled in a hollow waveguide. According to the calculations, the four-sided open waveguide beam has 50–3000 Hz transmission loss. Also, an experimental comparison was made to improve the work value (see Figure 43). The first six modes and natural frequencies were calculated and derived using the finite element software. Numerical results were validated with the experimental results. The results showed that the transmission losses in cubic and rectangular cubic structures with square and honeycomb unit cells for the absorbents in different directions differed slightly.

Huang and Sun⁴⁶ proposed and investigated a one-dimensional acoustic metadata structure for filtering waves. The cell used in this article is schematically shown in Figure 44—the present paper numerically simulated wave propagation in one-dimensional beams. The metamaterial was placed between two elastic environments to explore the propagation and filtering of the wave. The metamaterial test consisted of 12 single cells in the wave propagation direction. Each cell has 20 mm long. The 12 metamaterial cells were divided into four sections. The properties of each section were unique and different from another section.

For ease of operation and modeling, elastic environments on both sides of metamaterial were considered as a spring-mass system. In the first step, the wave spectrum was chosen to be out of bandwidth space. For this purpose, a spectrum with a central frequency of 3185 Hz and a frequency band between 2500 and 4100 Hz were applied to the set (including the first elastic medium, the metamaterial, and the second elastic medium). The results showed that almost all of the wave passed through the metamaterial without any change in shape and amplitude and reached the second elastic medium. The small amount of reflection was due to the slight difference in the impedance of the two environments. Next, the wave spectrum was selected to cover the frequency of the bandwidths. Therefore, a spectrum with a central frequency of 5900 Hz and a frequency band between 7900 and 4100 Hz were generated. The results were

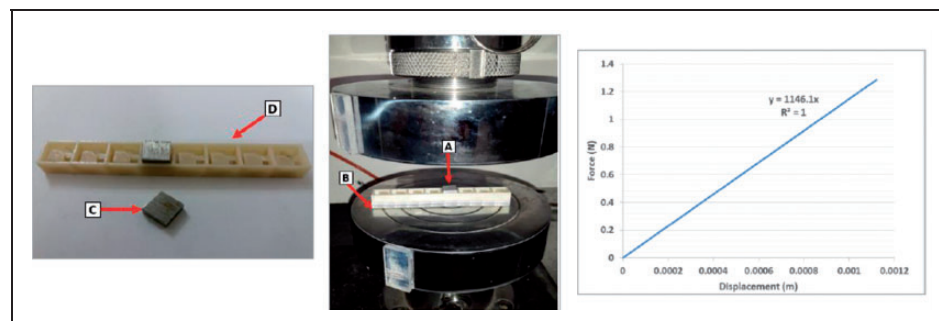


Figure 42. Measuring mechanical properties by experimental test, metamaterial unit cell, and force-displacement curve.⁴⁴

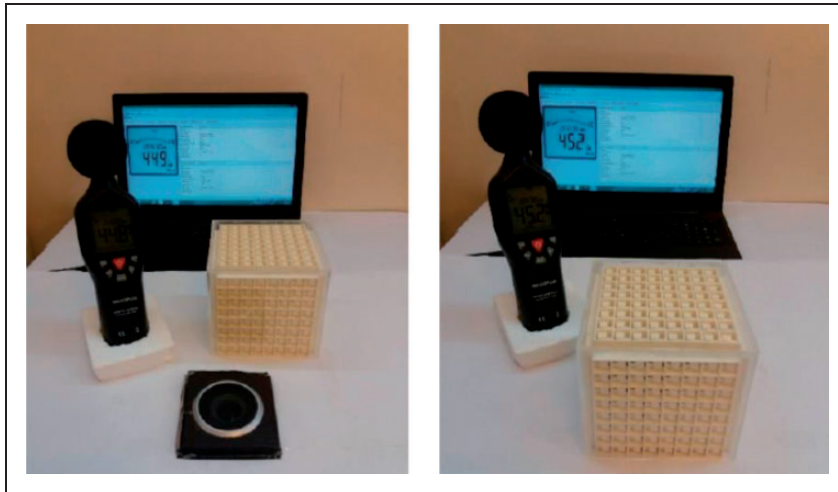


Figure 43. Experimental setting for measuring the frequency of the generated sound.⁴³

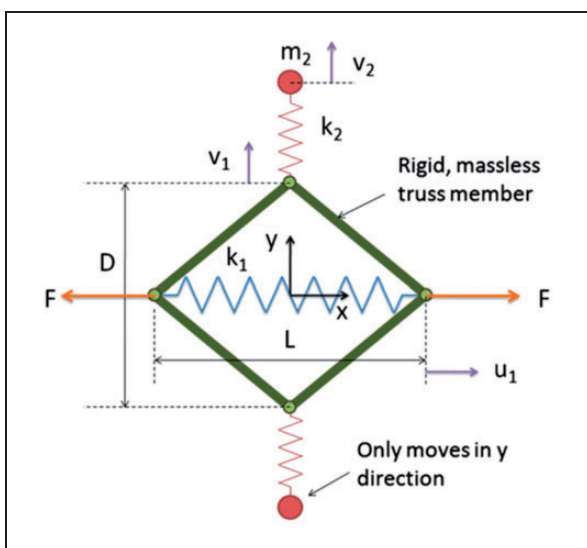


Figure 44. The one-dimensional cell for acoustic meta-structure.⁴⁵

recorded in the range of 0.005–0.05 s. In this case, a large part of the reflected wave was observed, and a small volume of it was transmitted to the second elastic medium. The results showed that only waves with the frequency equal to the resonance frequency of the metamaterial could pass through it and transfer to the second elastic medium.

Jing et al.⁴⁷ considered the metamaterial with zero indexes. The near-zero index refers to the environment with large phase velocity and wavelength. In other words, the wave in such an environment does not undergo any phase change. In the environment with a near-zero index, only the perpendicular waves are transmitted, and the rest of the waves are fully reflected. In their effort, they investigated membrane metamaterials and showed that the effective metamaterial density was close to zero around the membrane resonance frequency, which resulted in almost infinite

phase velocity and near-zero index. The introduced metamaterial consisted of several cells. Each cell consisted of four membranes that surround the air inside of themselves. The left side metamaterial was the free environment, and the other three were the non-reflective environment (Figure 45).

The wave was then transmitted to the metamaterial at two different frequencies with angles between 0° and 45° from the left side. These two frequencies included the resonant frequency of the membrane and the other arbitrary frequency. The displacements were recorded at the desired point within the membrane. At the resonant frequency, a high amplitude was recorded for the angle perpendicular to the surface, while for other angles, the amplitude of the oscillation decreased rapidly to zero. At non-resonant frequency, the amplitude did not change much at different angles. It occurred because, by increasing frequency, the index deviates from infinity. The results showed that only around the metamaterial resonance frequency, regular waves penetrated the structure. Such structure was introduced as the waves' angular filter. One of the new aspects is the appearance of metamaterials with the gradient refractive index. The specific geometry of these materials would reduce the speed and trap the acoustic waves. A series of slots perforated in a strip was embedded in these materials to localize the various frequency components and trap the broadband acoustic waves. Due to the similarity of the frequency resolution, these types of materials were called acoustic rainbow traps. Metamaterials that their modulus and density were anisotropic and had a refractive index much more considerable than air with gradual change could shorten the acoustic wavelength and concentrate its energy in a small area of a conical plate or a perforated array with tilt groove depth.

Dispersive AMs have been studied by Xinjing et al.⁴⁸ The process of absorbing a specific part of the sound waves by these metamaterials, compressing

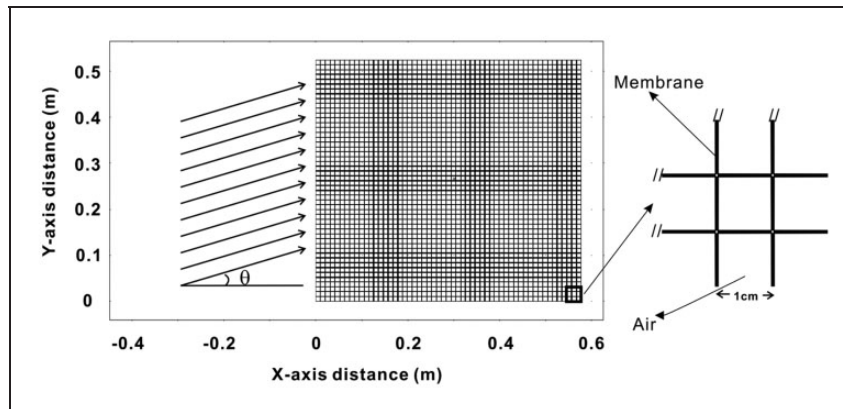


Figure 45. Metamaterial with several cells.⁴⁶

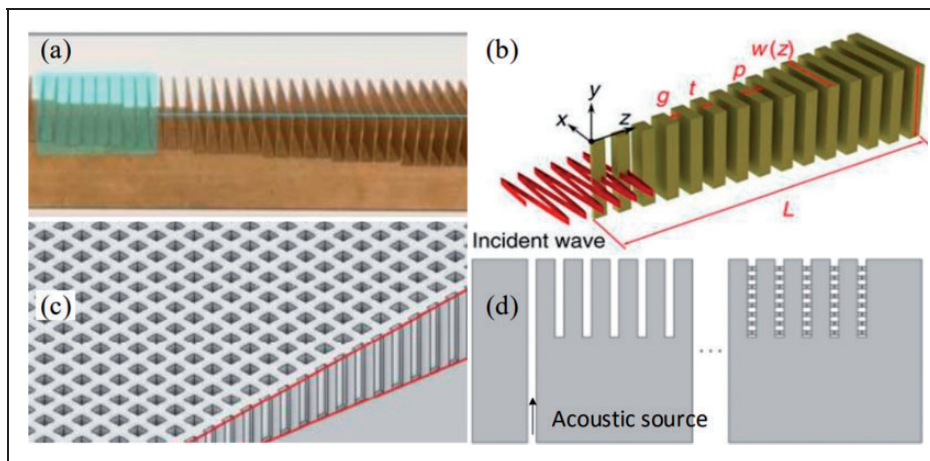


Figure 46. Four classic acoustic metamaterial models with graded grooves as well as rainbow trapping effect.⁴⁷

and amplifying the sound waves longitudinally within the metamaterials, and concentrating a particular frequency at a position in the metamaterial led to an effect called the rainbow trap. Figure 46 shows a summary of some conventional schemes of these materials and the rainbow trap effect. The present article has improved the layout of common metamaterials in several areas. First, the cross-section was changed to fit the dimensions of the cross-section in each distance. Second, the surface profile was changed from linear to nonlinear, and the gap between the plate and the thickness of the plate was decreased concurrently. It caused the heat to lose due to the viscosity effects of air inside of the gap. Figure 47 shows the introduced metamaterial.

The wave velocity decreased while propagating inside the metamaterial and stopped at specific locations, resulting in wave spatial-spectral separation in the space gaps. If the acoustic oscillations in the adjacent joints and the grooves were disturbed, the acoustic trapped rainbow would be released. The frequency that was further amplified was called the working frequency, and its value per groove decreased with increasing depth of the groove, thereby reducing the

metamaterial size to move the operating frequencies to higher values.

A novel kind of high sound transmission low was introduced by Ma et al.⁴⁹ To investigate the ability of the metamaterials to divide the signals into multiple frequencies, sound waves were received once by a single microphone without metamaterial and again by three microphones at three different points inside the metamaterial. The results showed that the signal of a particular frequency was amplified at each point within the metamaterial, and the frequency of other signals did not increase. One of the metamaterial applications is the removal of a specific frequency from the propagated wave. This work examined a novel method for eliminating a particular frequency from the wave. For this purpose, the interaction between the resonance frequency field of membrane metamaterial and the continuous frequency of the propagated wave was used. The tool introduced in their research consisted of one orifice in the center and four cells on the sides. Each cell comprised a circular membrane with a small thickness and a rigid disk attached to the middle of the membrane as an exciter. Each cell was attached to the screen

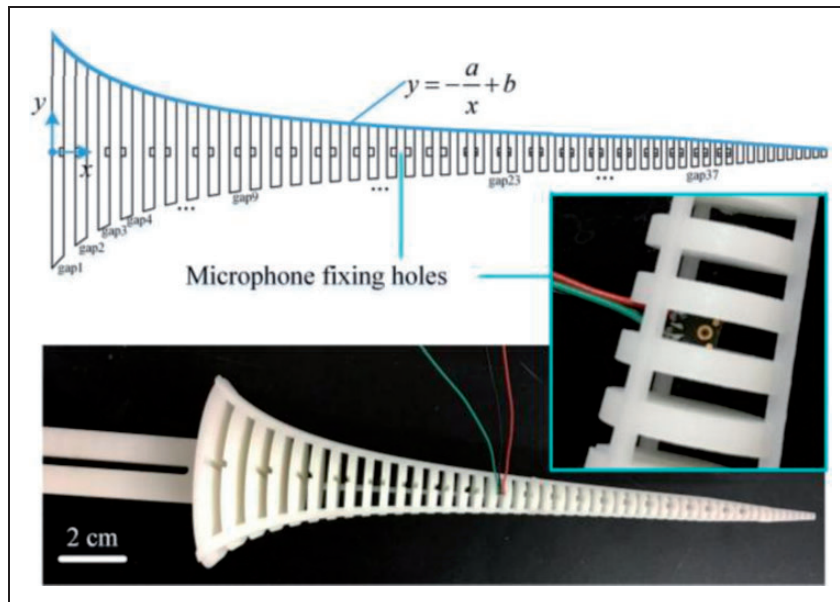


Figure 47. Proposed axial-symmetric acoustic metamaterial apparatus with inserted microphones in each gap, which has a gradient outline and a graded refractive index distribution.⁴⁷

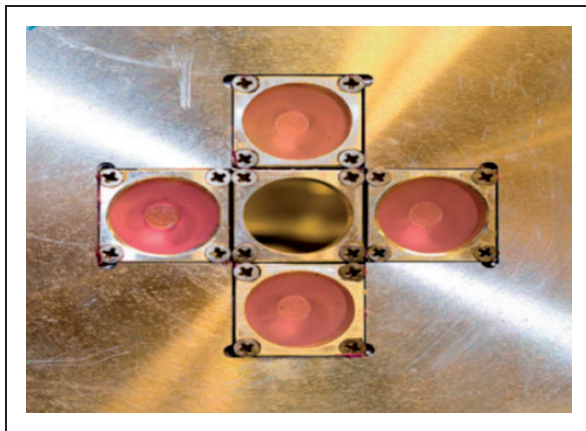


Figure 48. Tunable introduced a membrane-based device.⁴⁸

by a preload. By changing the excitation mass, the resonance frequency would be tunable. The system is introduced as shown in Figure 48.

The sound generator was positioned in front of the orifice, and two devices for measuring wave intensity were embedded along with it. The frequency diagram of the transmission coefficient of the device was plotted. The diagram included a minimum with a steep slope at 326 Hz and a maximum at 355 Hz. By blocking the aperture of each cell, the low frequency increased. The sharp drop in the transmission coefficient was due to the effects of the cells around the orifice. The transient properties of the device were clearly due to the diagram's peak and the first resonance mode. Due to the high intensity of wave propagation, this metamaterial was able to resist just at around the resonant frequency. Only when the metamaterial resonance field was 180° as opposed to the

wave direction, the metamaterial could significantly reduce the transmitted wave. Figure 49 displays the membrane metamaterial vibration profile and the velocity distribution of air particles that were obtained in their research. In Figure 49(a) (355 Hz), the general wave was amplified, and in Figure 49(b) (326 Hz), the general wave was attenuated. The reason for this was the difference and similarity direction between the generated wave phase and the emitted sound field by membrane metamaterial and orifice, respectively.

The results showed that the metamaterial density was zero at the excitation frequency and negative at the lower frequencies.

Tunable and reconfigurable metamaterials

Tunable metamaterials are another class of metamaterials that contain active and passive compounds. The performance of passive parts cannot be changed after construction, but their performance can be changed after construction by controlling the active parts. Tunable metamaterial performance can be adjusted by thermal, optical, magnetic, mechanical, and electrical mechanisms. Bao and Cui⁵⁰ examined various tunable metamaterials and their applications. They first examined the tunable metamaterials in the terahertz and microwave frequency range and then introduced different types of programmable metamaterials. Programmable metamaterial holograms, programmable metamaterial imager, space-time programmable metamaterials, and programmable metamaterial communication systems were some types of them. Programmable metamaterials were

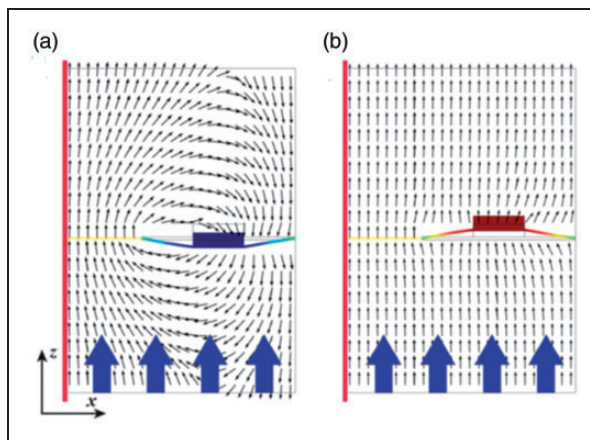


Figure 49. Vibration profile of the membrane metamaterial and velocity distribution of air particles.⁴⁸

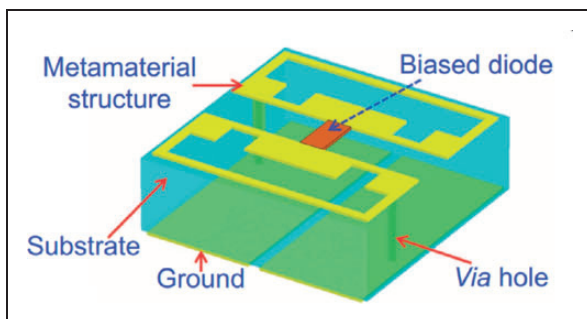


Figure 50. The first programmable metamaterial.⁴⁹

made up of controllable particles that were controlled by the field-programmable gate array. The first programmable metamaterial can be seen in Figure 50.

Bang et al.⁵¹ introduced various adjustment methods in tunable metamaterials and examined their improvements and defects. They described the role of thermal, electrical, optical, and mechanical effects in the regulation of metamaterials and showed that a stimulus could alter the single cells' arrangement in metamaterials and their properties. For example, the gold patterns on an elastic substrate could create meta-lens with variable properties and refractive index. A schematic of the introduced structure is displayed in Figure 51. According to this figure, the quadrangle elastic substrate was held by the arms. When force is applied to these arms, the substrate was stretched, and the distance between the specimens increased.

According to the above-mentioned research, materials whose properties change rapidly with temperature are suitable for use in tunable metamaterials. Although the thermal effect allows for an acceptable adjustment range for metamaterials, it may cause problems due to the time required for heating and cooling. Optical effects also have advantages that include tunability in the visible frequency range and compatibility with integrated circuits. The existence

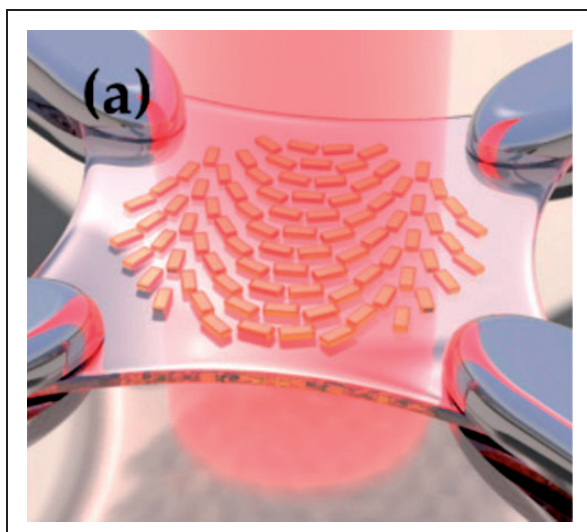


Figure 51. The schematic of tunable meta-lens.⁵⁰

of a narrow adjustable bandgap and the impossibility of adjusting all single cells is also one of the weaknesses of this method. With electromagnetic effects, the electromagnetic and mechanical properties of metamaterials can be changed and tuned. These methods include setting the parameters by adjusting the bandgap and controlling the current carriers in the substrate.

Photonic metamaterials

Photonic metamaterials are materials with high, low, or even negative refractive indexes that can manipulate optical waves in sub-wavelength dimensions. Iwanaga⁵² examined the photonic metamaterials using experimental studies and measured material parameters without assumptions. Electromagnetic resonance in photonic metamaterials was investigated using electromagnetic eigenmodes for two types of photonic metamaterials, including fishnet

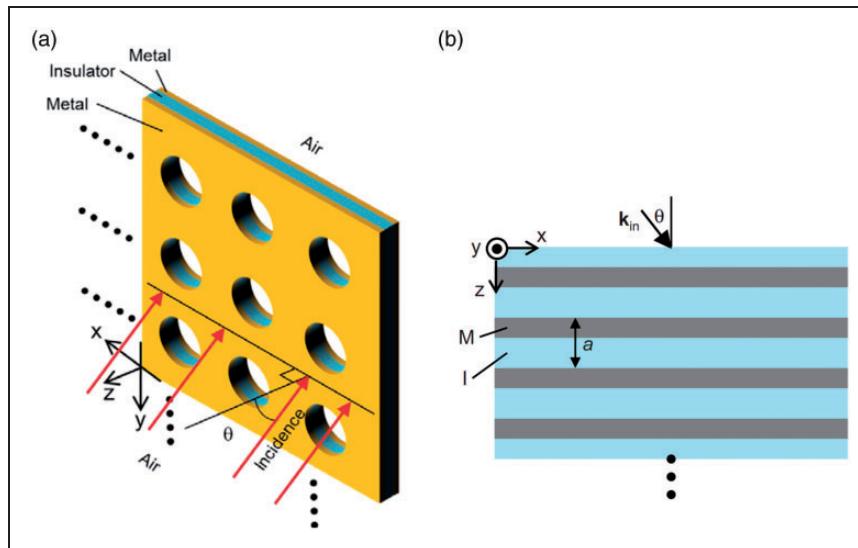


Figure 52. Two types of photonic metamaterials: (a) fishnet metamaterial slab; (b) 3D structure of stacked multilayer structure.⁵¹

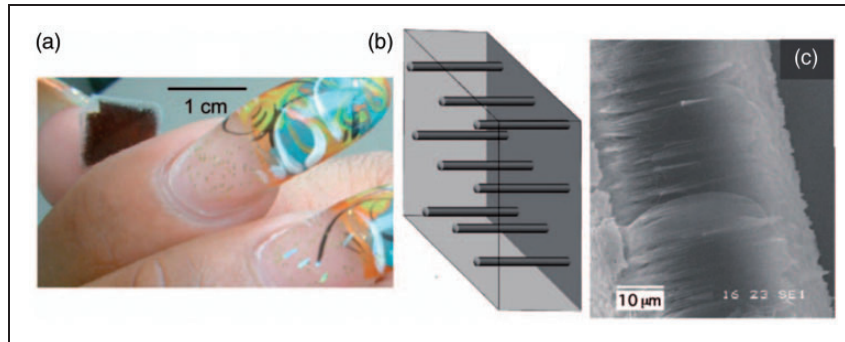


Figure 53. (a) Picture of the silver-filled membrane; (b) silver nanowires in an alumina membrane; (c) microscopic image of the lateral wall of the membrane.⁵²

metamaterial slab and 3D structure of stacked multilayer structure. Finally, the characteristics of both types of photonic metamaterials were specified without the need for specific models or assumptions. These two types of photonic metamaterial, which were examined, are shown in Figure 52(a) and (b).

Noginov et al.⁵³ designed the photonic metamaterial with hyperbolic dispersion. This material was the thickest photonic metamaterial made of silver-filled aluminum membranes. The properties of this material made it possible to use in imaging and optics. The designed metamaterial can be seen in Figure 53. This structure was three dimensional and had 15% porosity.

Frequency-selective surface-based metamaterial

Frequency-selective surfaces are a type of material with intermittent structures that act as the spatial filters. These materials transmit or reflect electromagnetic waves with different frequencies and radiations

and cause random and high-impedance surfaces or absorbers to be made. Due to limited space on practical applications, frequency selective surface-based metamaterials are used because the single cell in this type of structure has dimensions below the wavelength. In a review article, Wang et al.⁵⁴ elaborated frequency-selective surface-based metamaterials. They reviewed the basic design rules for this type of material and introduced various design theories. This type of material was then divided into two categories. They showed that dielectric materials, especially microwave ceramics, were good candidates for building frequency-selective surface-based metamaterials.

Fang et al.⁵⁵ created a stable metamaterial filter based on frequency selective surface. They theoretically and experimentally examined the transmission function of this structure and showed that by 90° rotation of the neighboring elements, the proposed structure had better stability for the polarization of longitudinal and transverse waves (see Figure 54).



Figure 54. Experimental test for measuring frequency-selective surface-based metamaterial.⁵⁴

Bandwidth setting of local resonance metamaterials

The need of adjustable bandgap in the structures that operate at different speeds has led to much research into metamaterials' tunability. Metastructures create some exciting properties, such as passbands and band gaps in their vibrational response. The frequency range in which local resonators allow vibrations to pass is called the bandwidth, and the range in which local resonators attenuate system vibrations is called the bandgap. Stop bands are divided into two types of Bragg bandgaps and local resonance bandgaps. Bragg bandgaps attenuate system vibrations in the high-frequency range. The local resonance bandgaps also control the frequency range of the system bandgaps locally. Memory alloys are a class of intelligent materials widely used to absorb or control flexible structures' vibrations. These materials are divided into two categories of one-way and two-way memory alloys. In one-way memory alloys, the modulus of elasticity increases with increasing temperature, and the phase of the material changes from martensite to austenite. In this type of memory alloy, the material is able to recover its shape in the austenite phase and returns to its original shape in the martensite phase using a base spring. The two-way memory alloys also form a curve with increasing temperature and return to their original shape with decreasing temperature without a base spring. In other words, two-way memory alloys can recover their shape at high and low temperatures and act as resonators with variable shapes and hardness. Although intelligent materials such as magnetic elastomers have been proposed for use in metamaterials, changes in mechanical properties due to magnetic or electric fields have imposed a limit on their use. Hu et al.¹⁸ analyzed the feasibility theory of the use of smart alloys (which are decomposed by cooling and return to their initial state after heating). The geometrical dimensions and the position of the absorbents

were investigated. Finally, a finite element relation was extracted based on the location of the absorbents on the beam. The results showed that by changing the smart alloys' mass and hardness by temperature, it was possible to shift the bandgap location and increase the bandwidth obtained in this method.

Sugino et al.⁵⁶ proposed a general theory for estimating bandwidth in one or two-dimensional vibrational structures. For estimating bandwidth, the differential operator formula was used, and an infinite number of resonators on the structure were considered. These resonators were tuned with the same frequency. This expression depended only on the extra mass ratio and the target frequency and did not depend on the boundary conditions of the structure. For the metamaterials with finite-dimensional local resonance and a limited number of resonators, approximating the total Riemann of an integral was used to estimate the bandwidth. The results showed that the optimal number of resonators for estimating bandwidth was directly related to the target frequency of the constant mass ratio. The bandwidth shown by the optimal number of resonators was wider than the bandwidth created by an infinite number of resonators, and these two values converged when the optimal number of resonators increased. The bandwidth corresponding with an unlimited number of resonators was compared with the bandwidth obtained by the plate wave method, and these results were in good agreement. One and two-dimensional structures with the corresponding resonators are depicted in Figure 55.

The experimental test was performed on a beam model that was made to confirm the theoretical results. The beam was made up of aluminum and had some resonators. The resonators were composed of steel springs and had a concentrated mass at their tip. The resonators were mounted on the beam at equal and non-equal distances, and experimental tests were performed on them. The corresponding experimental setup and arrangement are shown in Figure 56.

Because of the inability to switch different bandgap mechanisms in the conventional metamaterials, Chuang et al.⁵⁷ introduced a new set of metamaterials in which it was possible to switch the bandgap by using two-way curved shape memory alloys. The proposed metamaterials allowed two-way switching of bandgap between the local resonance and the Bragg scattering mechanisms. By reshaping and stiffening shape memory alloy resonators activated by heat processes, a reversible switch was made, and the metamaterial beam's bandgap mechanism was tuned. Typically, the resonators behaved like a PC beam. The bandgap was formed by an alternating array of concentrated masses. The concentrated masses were raised, and local resonance bandgap was formed by heating that was due to the curvature of shape memory alloy resonators. The

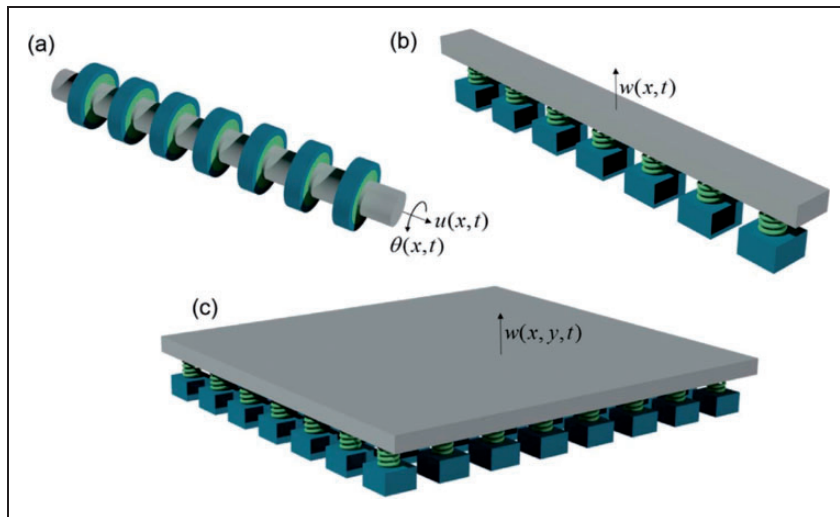


Figure 55. One and two-dimensional structures with corresponding resonators.⁵⁵

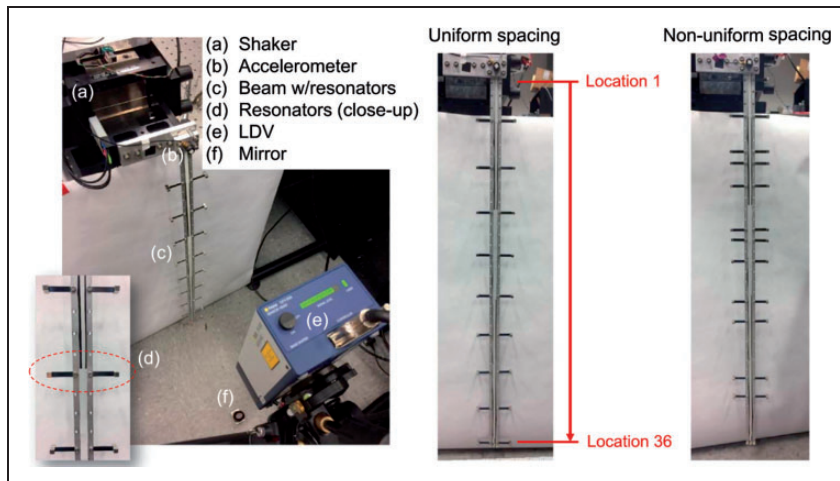


Figure 56. Experimental setup for vibrational testing of metamaterial beam.⁵⁵

theorem of Castigiano was used to obtain the equivalent spring stiffness of the curved beam. The calculated stiffness corresponded to the first two modes in two directions and validated the experimental results. Curved shape memory alloys were used instead of springs made of shape memory alloys to enhance local resonance bandwidth order. For tuning the negative effective mass density, the temperature of the heating process must be changed. As shown in Figure 57, the tunable elastic metamaterials could be understood by connecting an alternating array of curved resonators made of shape memory alloys. At the tip of each shape memory, the alloy was a steel ball. When this alloy was inactive, a PC was formed, and upon activation of the alloy, the resonator behaved as a spring-mass system. The steel ball and alloy were the mass and spring of each resonator, respectively.

Candido de Sousa et al.⁵⁸ tuned the bandwidth by changing temperature for a local resonance

metamaterial beam. Resonators were made of shape memory alloys, and their modulus of elasticity was a function of temperature. The properties of resonators were martensite at low temperature (for example, at room temperature) and austenitic at high temperature, which results in bandwidth transfer to lower and higher frequency bands, respectively. In this study, the effect of change of modulus of elasticity of resonators on bandgap at high temperature (austenitic phase) and low temperature (martensite phase) was investigated theoretically and experimentally. The results of the theory and experiments had a good agreement. By increasing the temperature from 25 to 45°C, the bandwidth and its lower range could be increased by 15%. This change could be controlled by the square root of the modulus of elasticity in the fully austenitic phase to a fully martensitic phase, and its values could be higher than 70% in other shape memory alloys. Figure 58 shows the corresponding experimental setup.

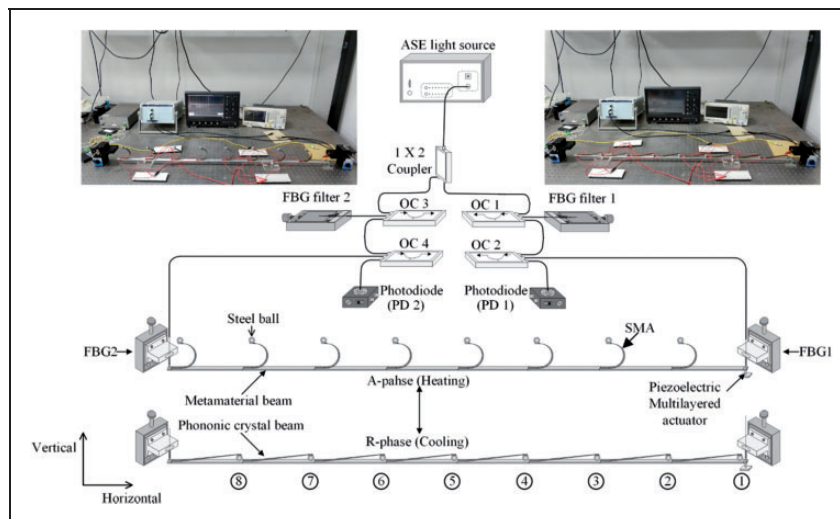


Figure 57. Experimental setting metamaterial and fiber-optic Bragg network displacement sensor system.⁵⁶

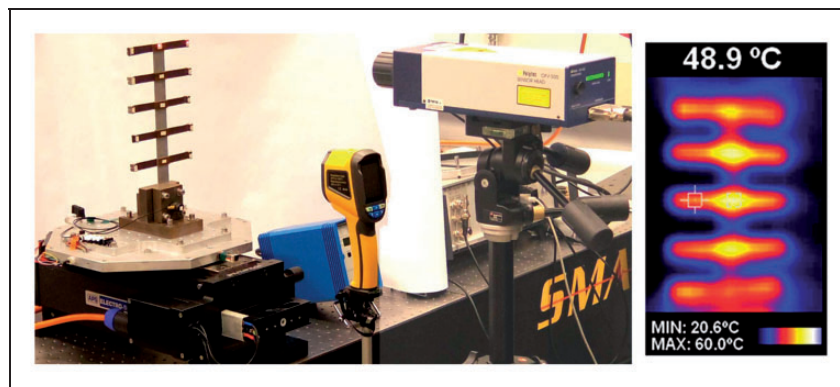


Figure 58. Experimental setup of bandgap in metamaterial beam.⁵⁷

Candido de Sousa et al.⁵⁹ tuned bandwidth in the local resonance metamaterials using shape memory alloy springs. The elastic modulus of the shape memory alloys was a function of temperature. Therefore, their properties changed between the martensite phase (low temperature) and austenitic phase (high temperature) due to the change in the natural frequencies of the resonators with the elastic modulus; the metamaterials can have a tunable bandgap. As the memory characteristics, materials were in their original shape retrieval after several times deformation due to external excitations such as heat. The shape memory alloys could act as exciter or spring. The exciter state was related to the memory effect, in which case the shape memory alloy became deformed by decreasing temperature and returned to its original form when the temperature was increased. This named the exciter state due to the bearing load by shape memory alloy. The spring state corresponds to a quasi-elastic effect, in which case the temperature was held up when the shape memory alloy was unloading and loading. Thus, by reducing the load, the original shape of the alloy is retrieved. The linear

or nonlinear behavior of the spring depended on the amount of stress applied to alloy in the quasi-elastic state. The results of this paper introduced a tunable bandgap in one- and multi-dimensional metamaterials with shape memory alloy resonators.

Zhou et al.² investigated the physical mechanism of negative affective parameters of metamaterials by introducing the spring, mass, and continuous versions of the metamaterial. After studying the mechanism of effective negative modulus, effective negative mass, and their interaction with macroscopic properties in a simple spring-mass system, they used the homogenization method to obtain the effective material properties of the continuous version of metamaterials. Hollow and rigid spheres attached by massless elastic springs provided a good structure for evaluating the negative effective mass mechanism. Figure 59 shows the corresponding structure.

The blockage effects on the negative effective mass frequency could be evaluated by measuring the transmission spectrum of the seven-unit lattice system. The experimental setup for measuring the transmission spectrum is displayed in Figure 60.

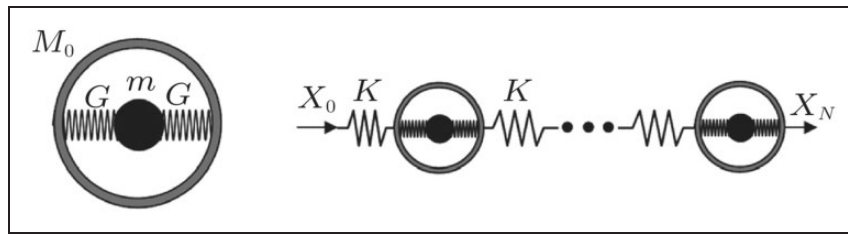


Figure 59. Mass-spring structure with effective negative mass.²

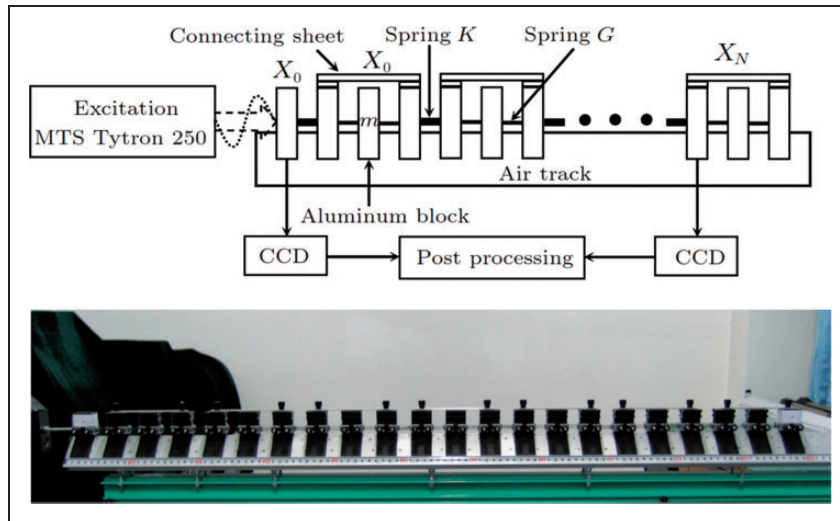


Figure 60. Experimental setting for measuring the transmission spectrum of the finite grid structure.²

They considered monopolar, dipolar, and quadrupolar resonances in composites with spheres coated in a solid matrix to design composites with negative bulk modulus, negative shear modulus, and effective negative mass. Homogenization theory was used to estimate the effective dynamic properties of the composite. The structure was under wave loading. The corresponding structure has been shown in Figure 61.

Yu et al.⁶⁰ studied the bandwidth of lateral vibrations of the Timoshenko beam. The position of the mentioned gap was calculated from the transfer matrix method, and the structural frequency response transfer was calculated from the finite element method. Most articles have used the frequency response of the structure to show the bandwidth position. Finally, the theoretical results were compared with the practical test results. The vibration of the structure was controlled by tuning the bandgap position. The metamaterial defined in the study was made of a hollow aluminum tube as a beam and a soft rubber ring and a copper ring as local actuators. The beam under test is depicted in Figure 62.

Initially, the end of the beam with a bandwidth of 0–800 Hz was excited. In this experiment, the beam was suspended by two straps so that it could vibrate freely. As mentioned, a beam head was excited by a

white noise absorber with a bandwidth of 0–800 Hz. In this article, the beam was considered to be a free end. An accelerometer measured the displacement of one end of the beam, and the frequency response of the other end was also extracted. Finally, the frequency response function (FRF) of the transmitted wave was measured by the B&K pulse system. The results showed that in the frequency band between 310 and 480 Hz, the frequency response was dropped below the range of the excitation frequency that this region indicated the bandgap of the structure.

Peng et al.⁶¹ introduced a multi-stop band metamaterial mechanism for elastic wave absorption and vibration suppression. Their metamaterial cell consisted of a plate as a base system integrating two-degree of freedom mass-spring subsystems, which act as the vibration absorbers (Figure 63). Due to the wider engineering applications of plates than bars and beams, their study focused on plate metamaterials. This article investigated the finite element model of the designed metamaterial. In their analysis, the first and second resonant frequencies of absorbers were assumed to be ideally equal. The vibration suppression performance of metamaterial was evaluated regarding the FRFs of the base plate without absorbers. The results showed that the first further damping of the absorber slightly widened the stopband to some

degree, although the large absorber damping led to increased transient time. On the other hand, large damping of the secondary absorber was induced by significant vibration suppression and a wider stopband.

The transient analysis showed that when the excitation happened inside the first stopband, the two absorbers moved-in phase, but 90° angles shifted from the base plate. In contrast, in the second stopband, the primary and secondary vibration absorbers worked out of phase whenever the plate and primary absorbers worked in an optical mode, and the plate and secondary absorbers worked in a mixed-mode, including optical and acoustic modes with a 90° shift phase.

Attarzadeh et al.⁶² worked on diode-like metamaterial to prevent back-scattered waves problem, limiting metamaterial application in many cases such as wave sensing. Their work designed an apparatus with time-dependent elastic modulus which could tune band gaps. The stiffness of apparatus local resonators varied by time through rotating their rectangular cross-sections. Metamaterial unit cells are composed of four resonator pairs with an assigned 45° spatial

phase shift in their cross-section angular orientation. All resonators rotated with a specific angular speed to produce the effective time-dependent stiffness. The experimental setup for the nonreciprocal elastic meta-beam is shown below in Figure 64.

The structure was tested at two quasi-static and dynamic regimes based on the rotational speed of CW and CCW rotations. A backward traveling material property wave appeared, moving from the end to the root of the beam with a CCW direction, while a CW direction results in moving from root to end. The results showed that the frequency shift of forward and backward-propagating branches was an integer multiple of temporal modulation frequency. The nonreciprocity could be strengthened by increasing the rotational speed. The one-way transmission at a given frequency could also be switched in the opposite direction by merely rotating motors in the opposite direction.

Hussein and Frazier⁶³ designed the periodic AMs with local resonance properties that showed high dissipation levels without decreasing stiffness or load-carrying capacity. They compared the AM characteristics with PC with the same long-wave propagation characteristics. Both systems had equal long-wave sound speed. By using Bloch's theorem, a mathematic formula was driven to represent the dispersion relation of AM and PC systems modeled by an infinite mass-spring chain. The results showed that although the AM bandgap was narrower than PC, the AM exhibited higher damping and higher dissipation across the entire Brillouin zone than the PC counterpart. It means that the attenuation of propagation across the entire spectrum was higher in AMs.

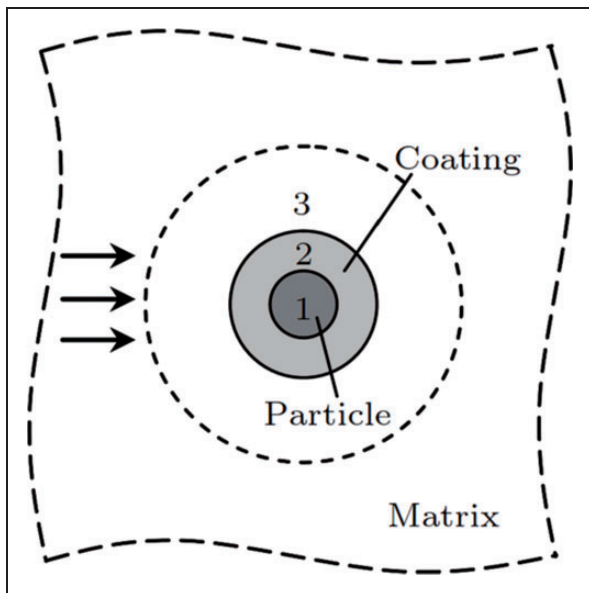


Figure 61. Analytical model of a sphere located in a solid matrix.²

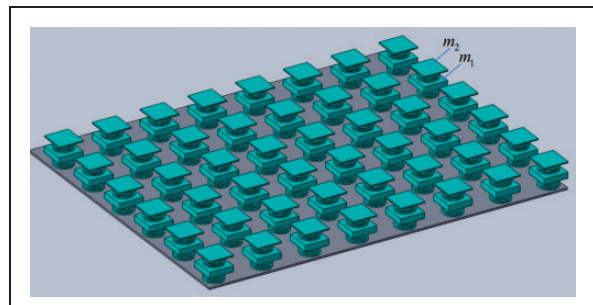


Figure 63. 3D view of the presented multi-stop band.⁶⁰

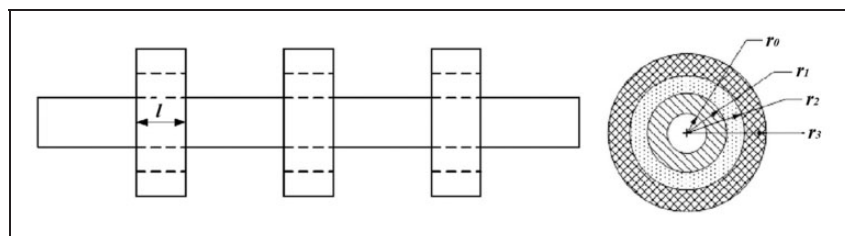


Figure 62. Picture of a Timoshenko beam used with local resonator.⁵⁹

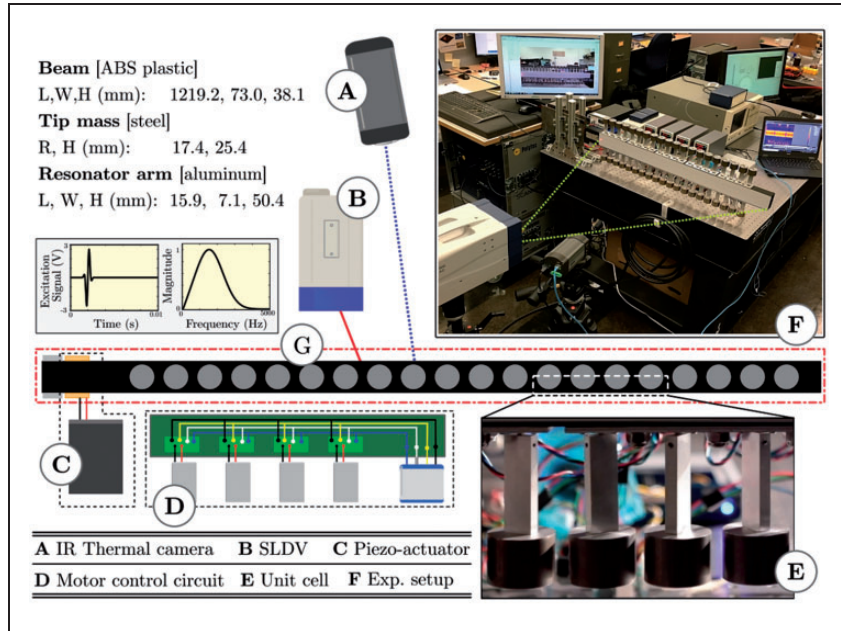


Figure 64. Experimental set-up for the elastic metabeam: (a) thermal imaging camera; (b) scanning laser doppler vibrometer imaging system; (c) beam excitation module and the signal sent to the piezoelectric actuator; (d) power and controller circuit; (e) unit cell (bottom half, close-up); (f, g) metabeam.⁶¹

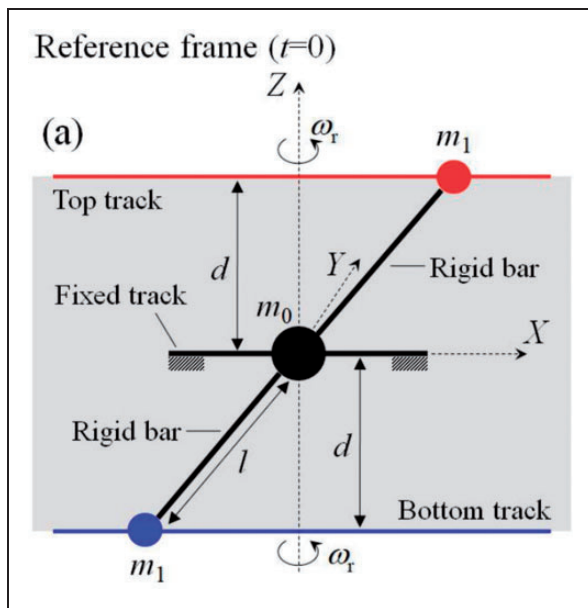


Figure 65. Illustration the diagram of the proposed metamaterial with time-varying inertial mass.⁶³

Moreover, AMs did not have a dependency between damping and stiffness, and the amplitude of dissipation in the AM enlarged without any effect on its stiffness. Huang and Zhuo⁶⁴ proposed a new dynamic metamaterial, which made wave propagation unidirectional. They introduced a rotational mechanism with a constant angular frequency consisted of three mass connected by two massless beams (Figure 65). By using Newton's law, an effective mass as a function of time was extracted.

Effective time-varying inertial mass was modified when motionless track and rotational tracks were unparalleled. A primary cell of the proposed metamaterial is shown in Figure 66. More than two primary cells with different angles were connected by spring to build a supercell. Constructed metamaterials were composed of repeated supercells. The phase difference between any two adjacent sub-cells did not change.

Bandgaps were split due to the time-driven mode interaction. One formed from the interaction of the 0th order and -1st order modes, while the other was the result of the interaction between the 0th and +1st orders. This led to the bandgaps that could only be observed in the forward direction due to the time-driven mode interaction. These arrangements would organize the bandgaps in the forward direction due to the time-driven mode interaction. In other words, only the backward wave was propagated at the bandgap frequencies. These results illustrated that the rotational frequency had a significant role in tuning the asymmetric gap frequency, and it would determine the central-frequency difference between the gaps and the direction of asymmetric bandgaps. Moreover, the bandwidth of the asymmetric bandgap would be enlarged by increasing the masses ratio.

Huang and Sun⁶⁵ examined how the bandgap changes by changing the parameters of the multi-resonator lattice system and drew the dispersion curve of it. Every single cell in the multi-resonator lattice system is made of three separate masses connected by the linear springs. The results showed that by changing the amplitude of the internal and constant mass of the spring, the bandwidth could be changed, and the effective mass equivalent of the

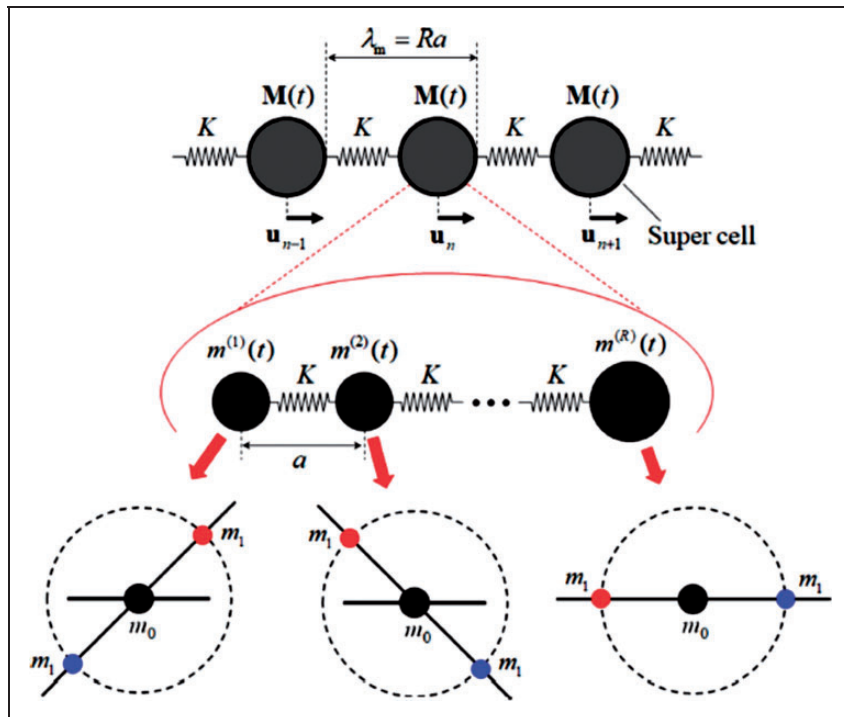


Figure 66. Schematic of the space-time lattice metamaterial composed of the time-varying mass and springs of constant stiffness K .⁶³

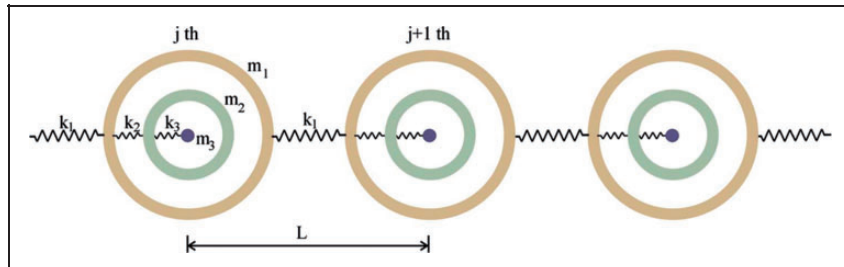


Figure 67. Dual resonator metamaterial system.⁶⁴

system would also be negative in the bandgap frequencies. Figure 67 shows the interconnected grid system.

Li et al.⁶⁶ designed a six-layer radial metamaterial shaft with arched layers, as shown in Figure 68. They extracted the eigenvalues of the system and determined the frequency response and dispersion curves by using the numerical method. The results showed that the designed system with a weight loss of 34% compared to the conventional metamaterial shafts could transmit the bandgap to the lower frequencies.

Meng et al.⁶⁷ fabricated a U-shaped metamaterial beam in which vibration absorbers were distributed in a rainbow pattern and separated by parallel plates. This structure was able to suppress the broadband vibrations. They examined the effect of mass distribution on the beam's frequency response by the analytical, numerical, and experimental methods. They showed that the beam's bandwidth was wider than the uniform mass distribution beam. The rainbow

metamaterial beam used in their study has been represented in Figure 69.

Sugino et al.²³ examined how the bandgap is distributed in the bimorph metamaterial beam with piezoelectric layers. Every single cell in the structure contained mechanical and electrical resonators that created the mechanical and electromechanical bandgaps. They defined the combined bandwidth size as a function of the ratio of the resonator mass and the level of an electromagnetic coupling system with an unlimited number of resonators. Finally, the dispersion curves were extracted using the plane wave expansion method. The results showed that in the absence of damping, mechanical and electromechanical bandgaps were always separate and did not combine. However, the presence of damping, although insignificant, would cause these bands to combine and facilitated the design of conventional systems. Figure 70 shows a bimorph beam with electromechanical resonators.

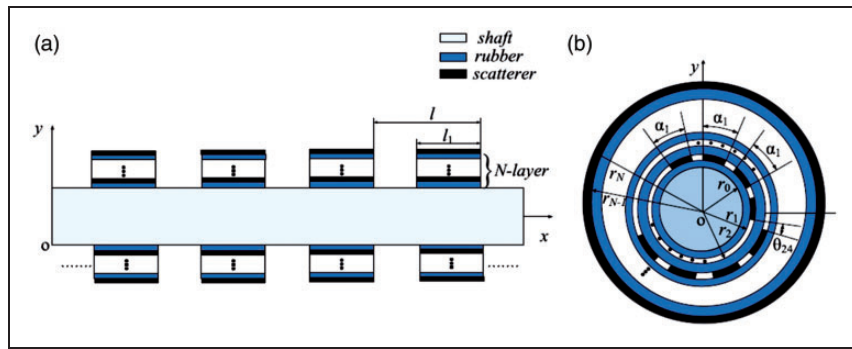


Figure 68. Metamaterial shaft and relevant unit cell.⁶⁵

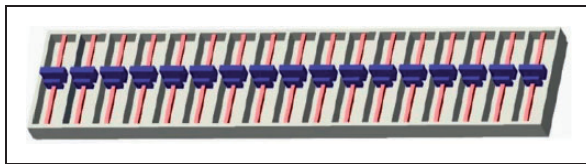


Figure 69. Rainbow metamaterial beam.⁶⁶

Yuan et al.⁶⁸ investigated the frequency response and the bandgap position in the two-layer interchangeable contact beam. Each unit cell of this structure consisted of four parallel elastic metal beams, ordinary springs, springs made of memory alloys, and magnets. With heat treatment, the spring phase of memory alloys was changed from martensite to austenite increasing their hardness and length. When the magnets were energized, repulsion or gravity would also be created between them. The magnets came into contact when the springs are long enough, and there was gravity between the magnets. They extracted the governing equations of the system motion and used the inverse matrix method to solve them. Then, they studied the effect of changes in stiffness and length of springs made of memory alloys, unit cell size, and energy amplitude applied to magnets on the bandwidth of the band. The results showed that the unit cell size and spring stiffness of memory alloys had a general effect on the bandwidth. Also, by changing the magnetic force and stiffness of ordinary springs, the band gap's width could be controlled locally. The accuracy of the data was verified when the results were compared with the numerical process. Figure 71 illustrates the composition of the metamaterial.

A new elastic metamaterial design was proposed based on the rack-and-pinion mechanism by Shirazi and Sedighi.⁶⁹ The design process included a fundamental model with a single resonator and a developed model with multiple rotational resonators (see Figure 72). The whole model system composed of an array of cells acting as the rack. Each cell included a pinion disk connected to the cell with a linear spring. The discrete proposed model predicted the optical mode

for a wide range of frequency domain. Moreover, using the rotational double-resonator metamaterial, the nonlinear effects were omitted by preventing moment effects between the masses and structures. Besides, the kinetic energy absorbed by this method was more than the translational double-resonator system. By using the proposed mechanism, two bandgap regions were tailored in which the width of the first bandgap was tunable by adjusting inner mass and moment of inertia, while the width of the second bandgap changed by outer mass and moment of inertia. The location of the bandgap could be determined by modulating spring stiffness and outer mass. It was demonstrated that when a portion of the frame mass and the spring stiffness were within the specific interval, the starting frequency of the second bandgap would be built wider bandgap, which had a tremendous demand for broadband vibration attenuation. The model was simulated and analyzed through MSC-ADAMS software to verify the numerical analysis, which showed acceptable agreement with the numerical method.

Ongoing research

As documented herein, periodic metamaterial systems offer exciting opportunities and unparalleled potential to influence fundamental studies and completely revolutionize the manufacturing of future technologies. For instance, a metamaterial-based absorber proposed by Alkurt et al.⁷⁰ has a dielectric as a substrate layer covered by a preventer copper plate. This innovative structure might be used as a microwave image detector, which removes noise, and cells are often utilized in various areas like energy harvesting, incident wave tracing, crack detection, spy device detection, and medical imaging.

A variety of lab methods are available to organize individual cells on large and small scales. There are benefits and drawbacks of both of these approaches. An experimental evaluation of these materials has been constrained by the fragility of metamaterials under tensile loading. In many studies, various methods are used based on the scale of the metamaterial

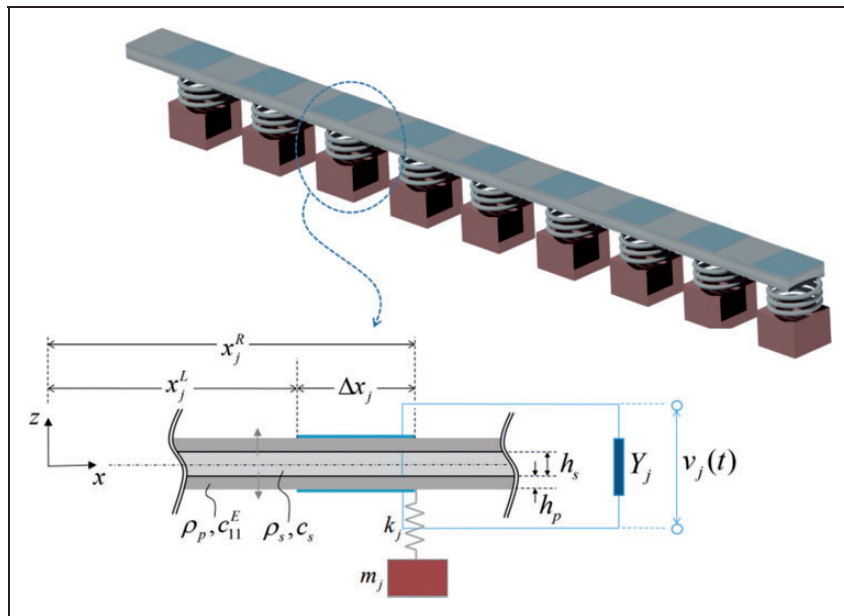


Figure 70. Bimorph beam with electromechanical resonators.²³

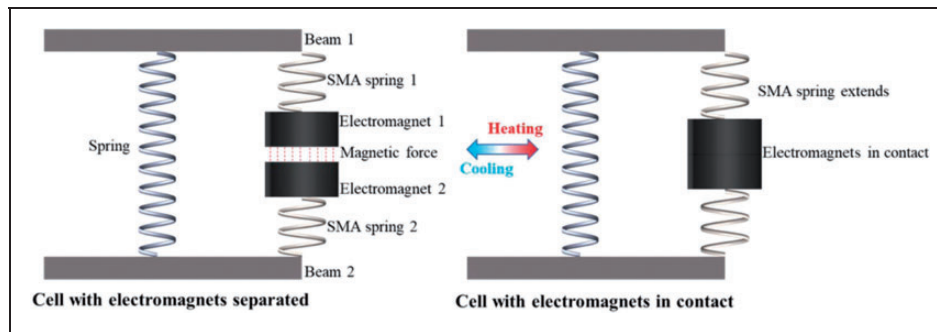


Figure 71. Metamaterial double-layer beam layout with contact switching capability.⁶⁷

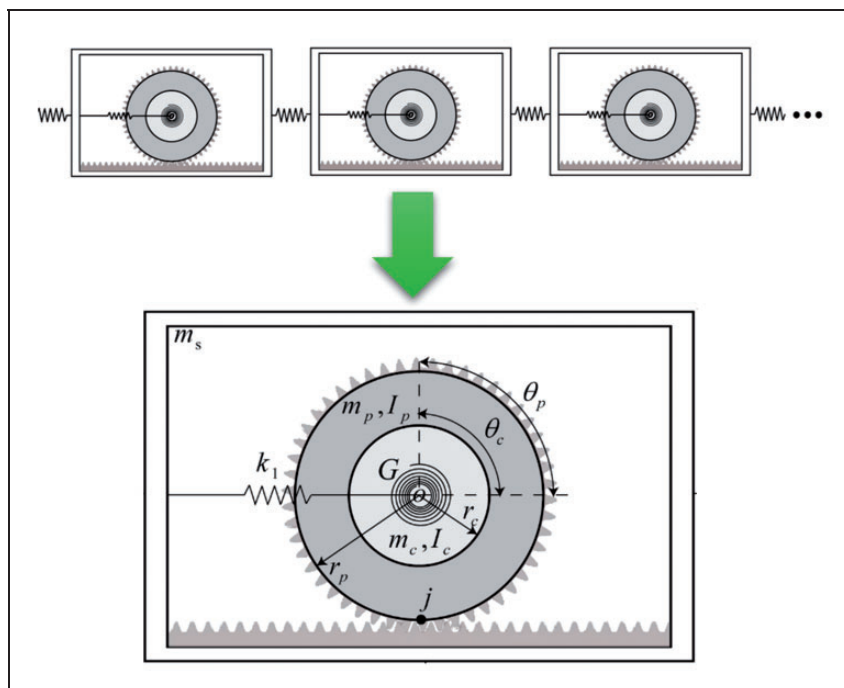


Figure 72. A schematic model of the proposed metamaterial and its unit cell.⁶⁸

Table 1. Different types of metamaterials and their corresponding features.

Type of metamaterial	Definition	Application	Advantage	Disadvantage
Piezoelectric	Periodic structure with piezoelectrics patch to control energy followed by converting mechanical and electrical energy to each other	● MEMS ● Sensors ● Wave guideline	● Flexible and tunable bandgaps ● Wide bandwidth	– Expensive – Sensitive to spatial changes
Electromagnetic	Use electrical and magnetic energy to manipulate the material properties periodically	● Smart Material ● MEMS ● Sound filtering ● Biosensors	● Wide range of bandwidth ● Tunable bandgap	– It needs a considerable amount of energy
Chiral	consist of arrays of planar metallic or dielectric	● Plasmonic devices	● Lightweight ● Enhanced mechanical properties	– Higher dimensions – Need 3D printer
Nonlinear	Metamaterial with nonlinear properties or geometries of each cell	● Super-resolution ● Strong local field enhancement	● Not need for any external stimulation	– Narrow bandgap – power dependency
Acoustic	Periodic structure designed to control, direct, and manipulate sound wave propagation	● NDT test ● Wave filtering ● Noise reduction	● Low-frequency elastic wave propagation. ● Sandwich panels	– Narrow frequency band
Photonic	Periodic structure designed to control, direct, and manipulate optical wave propagation	● Super Lens ● Optical wave manipulation	● Cost-effective	– Lack of tunability and flexibility – Undesirable loss
Terahertz	Novel high-intensity THz metamaterial interact at terahertz frequencies, usually defined as 0.1 to 10 THz	● Remote sensing ● Spectroscopy	● Controlling radiations in the terahertz regime	– Limits to propagating the terahertz band through the atmosphere – Heavy equipment

specimens. High-resolution multi-photon lithography allows metamaterial measurements at micron and sub-micron sizes.⁷¹

Most of the wave-type arguments for bandgap formation are based on moving waves' assumptions on an infinite structure made from a repeated unit cell and using symmetrical cell properties. Recently, however, a few studies on a number of cells have worked on finite structures. In El Sherbiny and Placidi,⁷² the minimum number of required resonators was pointed out to observe a clear bandgap. The simulations showed that the number of resonators should be at least equal to the mode shape number, which is the highest mode shape number gain from the based model without resonators and is included in the bandgap's frequency range. Moreover, they reported that downward changes in formed bandgap frequency would occur by decreasing the number of resonators. Sugino et al.⁷³ showed that the required cells to establish a bandgap would increase as the desired frequency gets bigger. Their analysis revealed that raising the number of cells enhances the amplification reduction, and the bandgap size depends on the unit cell's total size.

Conclusions

Thanks to their exceptional properties, metamaterials are becoming a new and, of course, an interesting field of research for many scientists in different areas of science such as physics, engineering, mathematics, etc. Metamaterials have many types with additional features and applications, and their extraordinary properties cause them to be utilized in various fields and disciplines. Piezoelectric, electromagnetic, terahertz, acoustics, absorbers, frequency selective surface-based metamaterials, and nonlinear ones are different kinds of metamaterials. General safety, sensor identification, high-frequency battlefield communications, improved ultrasonic sensors, solar energy management for high-gain antennas, metamaterial-enhanced magnetic induction, and remote aerospace are several applications of metamaterials. Some critical challenges about metamaterial-enhanced magnetic induction design are the construction of spherical metamaterials, control of effective parameters, and the need for more considerable transmission distances than antenna size. Another application of metamaterials is magnetic field protection. Magnetic field protection in materials with high permeability is based on guiding or trapping the magnetic field and in materials with low permeability is done by repelling the magnetic field. Magnetic field protection is also improved when a non-isotropic material with different permeability coefficients in different directions is used. Bandwidth setting in metamaterials is a fundamental issue that has been considered nowadays. Metastructures exhibit some exciting properties such

as passbands and band gaps in their vibrational response. The frequency range in which local resonators allow vibrations to pass is called the bandwidth. The range in which local resonators attenuate the vibrations of the system is called the bandgap. Stopbands are divided into two types of Bragg bandgaps and local resonance bandgaps. Bragg bandgaps attenuate the vibrations of the system in the high-frequency range. The local resonance bandgaps also control the frequency range of system bandgaps locally. The fragility of metamaterials against tensile loads has limited the experimental test of these materials. Depending on the size of the metamaterial specimens, different tools are used for testing. Studies on metamaterials are mostly related to the quasi-static states, although dynamic conditions are rarely studied. The metamaterial structure concept with damp vibrations is based on embedding the local resonance systems into a single-cell structure. The resulting alternating structure can be treated as a material with dynamic properties to be exploited in various engineering fields. In this review article, an overview of different analyses performed on the multiple metamaterials together with their applications was comprehensively provided. Other types of metamaterials and their different modeling methods were also presented. Finally, a review of researches in the field of bandgap setting in the local resonance metamaterials was considered and discussed. Finally, in order to suitably summarize the contents of this review article, Table 1 presented different kinds of metamaterials together with their application, advantages, and disadvantages.

Declaration of conflicting interests

The author(s) declared no potential conflicts of interest concerning the research, authorship, and publication of this article.

Funding

The author(s) disclosed receipt of the following financial support for the research, authorship, and/or publication of this article: Research Council of the Shahid Chamran University of Ahvaz for its financial support (Grant No. SCU.EM99.98).

ORCID iD

Hamid M Sedighi  <https://orcid.org/0000-0002-3852-5473>

References

1. Hussein MI, Leamy MJ and Ruzzene M. Dynamics of phononic materials and structures: historical origins, recent progress, and future outlook. *Appl Mech Rev* 2014; 66: 040802.
2. Zhou X, Liu X and Hu G. Elastic metamaterials with local resonances: an overview. *Theor Appl Mech Lett* 2012; 2: 041001.
3. Apaydin N, Sertel K and Volakis JL. Nonreciprocal leaky-wave antenna based on coupled microstrip lines

- on a non-uniformly biased ferrite substrate. *IEEE Trans Antennas Propag* 2013; 61: 3458–3465.
4. Hu G. Metastructure with piezoelectric element for simultaneous vibration suppression and energy harvesting. *J Vib Acoust* 2016; 139: 011012.
 5. Erb RM, Libanori R, Rothfuchs N, et al. Composites reinforced in three dimensions by using low magnetic fields. *Science* 335; 2012: 199.
 6. Courjal N, Bernal MP, Ulliac G, et al. LiNbO₃ acousto-optical and electro-optical micromodulators. *J Eur Opt Soc* 2009; 4: 09018.
 7. Shen SH, Fang W and Young ST. Design considerations for an acoustic MEMS filter. *Microsyst Technol* 2004; 10: 585–591.
 8. Bisoffi M, Hjelle B, Brown DC, et al. Detection of viral bioagents using a shear horizontal surface acoustic wave biosensor. *Biosens Bioelectron* 2008; 23: 1397–1403.
 9. Li WH and Zhang XZ. A study of the magnetorheological effect of bimodal particle based magnetorheological elastomers. *Smart Mater Struct* 2010; 19: 35002.
 10. Xu ZB, Gong XL, Liao GJ, et al. An active damping compensated magnetorheological elastomer adaptive tuned vibration absorber. *J Intell Mater Syst Struct* 2010; 21: 1039–1047.
 11. Hofmann T, Helbig T, Schindler F, et al. Reciprocal skin and its realization in a topoelectrical circuit. *arXiv Prepr* 2019; 2: 023265.
 12. Singh G and Marwaha A. A review of metamaterials and its applications. *Int J Eng Trends Technol* 2015; 19: 305–310.
 13. Banerjee B. *An introduction to metamaterials and waves in composites*. Boca Raton, FL: CRC Press, 2011.
 14. Schürch P and Philippe L. *Composite metamaterials: types and synthesis. Reference module in materials science and materials engineering*. Amsterdam, Netherlands: Elsevier, 2021.
 15. Fok L, Ambati M and Zhang X. Acoustic metamaterials. *MRS Bull* 2008; 33: 931–934.
 16. Khan K, Al-Mansoor S, Khan S, et al. Piezoelectric metamaterial with negative and zero Poisson's ratios. *J Eng Mech* 2019; 145: 04019101.
 17. Zhu R, Chen YY, Barnhart MV, et al. Experimental study of an adaptive elastic metamaterial controlled by electric circuits. *Appl Phys Lett* 2016; 108: 011905.
 18. Hu H-L, Peng J-W and Lee C-Y. Dynamic simulation of a metamaterial beam consisting of tunable shape memory material absorbers. *Vibration* 2018; 1: 81–92.
 19. Chen YY, Zhu R, Barnhart MV, et al. Enhanced flexural wave sensing by adaptive gradient-index metamaterials. *Sci Rep* 2016; 6: 1–11.
 20. Matlack KH, Bauhofer A, Krödel S, et al. Composite 3D-printed metastructures for low frequency and broadband vibration absorption. *Proc Natl Acad Sci USA* 2016; 113: 8386–8390.
 21. Nouh MA, Aldraihem OJ and Baz A. Periodic metamaterial plates with smart tunable local resonators. *J Intell Mater Syst Struct* 2016; 27: 1829–1845.
 22. Popa BI, Shinde D, Konneker A, et al. Active acoustic metamaterials reconfigurable in real time. *Phys Rev B* 2015; 91: 220303.
 23. Sugino C, Ruzzene M and Erturk A. Merging mechanical and electromechanical bandgaps in locally resonant metamaterials and metastructures. *J Mech Phys Solids* 2018; 116: 323–333.
 24. Mendhe SE and Kosta YP. Metamaterial properties and applications. *Int J Inform Technol Knowldg Manage* 2011; 4: 85–89.
 25. Magnus F, Wood B, Moore J, et al. A DC magnetic metamaterial. *Nat Mater* 2008; 7: 295–297.
 26. Guo H, Sun Z and Zhou C. Practical design and implementation of metamaterial-enhanced magnetic induction communication. *IEEE Access* 2017; 5: 17213–17229.
 27. Boyvat M and Hafner CV. Molding the flow of magnetic field with metamaterials: magnetic field shielding. *Prog Electromagn Res* 2012; 126: 303–316.
 28. Ali H, Forsberg E and Jun H. Brain imaging with slotted hybridized magnetic metamaterial hat at 7-T MRI. *Appl Magn Reson* 2017; 48: 67–83.
 29. Abirami N and Wilson KJ. Analysis of properties of metamaterial-based composite system. *Int J Mod Phys B* 2019; 33: 1950154.
 30. Chen Z, Chen S, Wang Y, et al. Tunable atom-trapping based on a plasmonic chiral metamaterial. *Nanophotonics* 2019; 8: 1739–1745.
 31. Sabah C, Dincer F, Karaaslan M, et al. Biosensor applications of chiral metamaterials for marrowbone temperature sensing. *J Electromagn Wave Appl* 2015; 29: 2393–2403.
 32. Zhu R, Liu X, Hu G, et al. A chiral elastic metamaterial beam for broadband vibration suppression. *J Sound Vib* 2014; 333: 2759–2773.
 33. Wu W, Hu W, Qian G, et al. Mechanical design and multifunctional applications of chiral mechanical metamaterials: a review. *Mater Des* 2019; 180: 107950.
 34. Gangwar K, Paras and Gangwar RPS. Metamaterials: characteristics, process and applications. *Adv Electron Electr Eng* 2014; 4: 97–106.
 35. Landy NI, Sajuyigbe S, Mock JJ, et al. Perfect metamaterial absorber. *Phys Rev Lett* 2008; 100: 207402.
 36. Hossain MJ, Faruque MRI and Islam MT. Perfect metamaterial absorber with high fractional bandwidth for solar energy harvesting. *PloS One* 2018; 13: e0207314.
 37. Tran MC and Phuong TTH. Two-layered dual-band perfect metamaterial absorber at K band frequency. *Adv Electromagn* 2018; 7: 25–27.
 38. Xie J, Zhu W, Rukhlenko ID, et al. Water metamaterial for ultra-broadband and wide-angle absorption. *Opt Exp* 2018; 26: 5052–5059.
 39. Gao M, Wu Z and Wen Z. Effective negative mass nonlinear acoustic metamaterial with pure cubic oscillator. *Adv Civ Eng* 2018. DOI: 10.1155/2018/3081783.
 40. Cveticanin L and Zukovic M. Negative effective mass in acoustic metamaterial with nonlinear mass-in-mass subsystems. *Commun Nonlinear Sci Numer Simul* 2017; 51: 89–104.
 41. Khajehtourian R and Hussein MI. Dispersion characteristics of a nonlinear elastic metamaterial. *AIP Adv* 2014; 4: 124308.
 42. Xia Y, Ruzzene M and Erturk A. Dramatic bandwidth enhancement in nonlinear metastructures via bistable attachments. *Appl Phys Lett* 2019; 114: 093501.
 43. Asgari S, Sharifi N and Granpayeh N. Active tunable terahertz micro-electromechanical metamaterial absorber. *J Micromech Microeng* 2019; 29: 045010.

44. Hu G, Tang L, Das R, et al. Acoustic metamaterials with coupled local resonators for broadband vibration suppression. *AIP Adv* 2017; 7: 025211.
45. Ebrahimi-Nejad S and Kheybari M. Honeycomb locally resonant absorbing acoustic metamaterials with stop band behavior. *Mater Res Exp* 2018; 5: 105801.
46. Huang HH and Sun CT. Theoretical investigation of the behavior of an acoustic metamaterial with extreme Young's modulus. *J Mech Phys Solid* 2011; 59: 2070–2081.
47. Jing Y, Xu J and Fang NX. Numerical study of a near-zero-index acoustic metamaterial. *Phys Lett Sect A Gen At Solid State Phys* 2012; 376: 2834–2837.
48. Xinjing H, Yutian Y, Jinyu M, et al. An acoustic metamaterial-based sensor capable of multiband filtering and amplification. *IEEE Sens J* 2020; 20: 4413–4419.
49. Ma A, Zhong R, Wu Z, et al. Ultrasensitive THz sensor based on centrosymmetric F-shaped metamaterial resonators. *Front Phys* 2020; 8: 1–7.
50. Bao L and Cui TJ. Tunable, reconfigurable, and programmable metamaterials. *Microw Opt Technol Lett* 2020; 62: 9–32.
51. Bang S, Kim J, Yoon G, et al. Recent advances in tunable and reconfigurable metamaterials. *Micromachines* 2018; 9: 560.
52. Iwanaga M. Photonic metamaterials: a new class of materials for manipulating light waves. *Sci Technol Adv Mater* 2012; 13: 053002.
53. Noginov M, Barnakov YA, Zhu G, et al. Bulk photonic metamaterial with hyperbolic dispersion. *Appl Phys Lett* 2009; 94: 151105.
54. Wang J, Qu S, Li L, et al. All-dielectric metamaterial frequency selective surface. *J Adv Dielectr* 2017; 7: 1730002.
55. Fang C, Gao J and Liu H. A novel metamaterial filter with stable passband performance based on frequency selective surface. *AIP Adv* 2014; 4: 077114.
56. Sugino C, Xia Y, Leadenham S, et al. A general theory for bandgap estimation in locally resonant metastructures. *J Sound Vib* 2017; 406: 104–123.
57. Chuang K-C, Lv X-F and Wang Y-H. A bandgap switchable elastic metamaterial using shape memory alloys. *J Appl Phys* 2019; 125: 055101.
58. Candido de Sousa V, Tan D, De Marqui C Jr, et al. Tunable metamaterial beam with shape memory alloy resonators: theory and experiment. *Appl Phys Lett* 2018; 113: 143502.
59. de Sousa VC, Sugino C, Junior CM, et al. Adaptive locally resonant metamaterials leveraging shape memory alloys. *J Appl Phys* 2018; 124: 064505.
60. Yu D, Liu Y, Wang G, et al. Flexural vibration band gaps in Timoshenko beams with locally resonant structures. *J Appl Phys* 2006; 100: 124901.
61. Peng H, Pai PF and Deng H. Acoustic multi-stop band metamaterial plates design for broadband elastic wave absorption and vibration suppression. *Int J Mech Sci* 2015; 103: 104–114.
62. Attarzadeh MA, Callanan J and Nouh M. Experimental observation of nonreciprocal waves in a resonant metamaterial beam. *Phys Rev Appl* 2020; 13: 021001.
63. Hussein MI and Frazier MJ. Metadamping: an emergent phenomenon in dissipative metamaterials. *J Sound Vib* 2013; 332: 4767–4774.
64. Huang J and Zhou X. A time-varying mass metamaterial for non-reciprocal wave propagation. *Int J Solids Struct* 2019; 164: 25–36.
65. Huang G and Sun C. Band gaps in a multiresonator acoustic metamaterial. *J Vib Acoust* 2010; 132: 031003.
66. Li L, Lv R, Cai A, et al. Low-frequency vibration suppression of a multi-layered elastic metamaterial shaft with discretized scatters. *J Phys D: Appl Phys* 2018; 52: 055105.
67. Meng H, Chronopoulos D and Fabro AT (eds) A rainbow metamaterial for broadband multi-frequency vibration suppression. In: *INTER-NOISE and NOISE-CON congress and conference proceedings*, InterNoise19, Madrid, Spain, 2019.
68. Yuan Y, Li J, Bao R, et al. A double-layer metastructured beam with contact-separation switchability. *Mech Adv Mater Struct*. Epub ahead of print 17 August 2020. DOI: 10.1080/15376494.2010.1804017.
69. Shirazi AH and Sedighi HM. Physics of rack-and-pinion-inspired metamaterials with rotational resonators for broadband vibration suppression. *Eur Phys J Plus* 2020; 135: 1–23.
70. Alkurt FO, Altintas O, Ozakturk M, et al. Enhancement of image quality by using metamaterial inspired energy harvester. *Phys Lett A* 2020; 384: 126041.
71. Fischer SC, Hillen L and Eberl C. Mechanical metamaterials on the way from laboratory scale to industrial applications: challenges for characterization and scalability. *Materials* 2020; 13: 3605.
72. El Sherbiny MG and Placidi L. Discrete and continuous aspects of some metamaterial elastic structures with band gaps. *Arch Appl Mech* 2018; 88: 1725–1742.
73. Sugino C, Leadenham S, Ruzzene M, et al. An investigation of electroelastic bandgap formation in locally resonant piezoelectric metastructures. *Smart Mater Struct* 2017; 26: 055029.